TÜBİTAK

Turkish Journal of Earth Sciences

http://journals.tubitak.gov.tr/earth/

Research Article

Turkish J Earth Sci
(2013) 22: 715-738

doi:10.3906/yer-1206-7

Cenozoic tectonics of the Tuz Gölü Basin (Central Anatolian Plateau, Turkey)

David FERNÁNDEZ-BLANCO[1,*], Giovanni BERTOTTI[1,2], T. Attila ÇİNER[3]

[1]Tectonics and Structural Geology Department, Faculty of Earth and Life Sciences, Vrije Universiteit, Amsterdam, the Netherlands
[2]Department of Geotechnology, Faculty of Civil Engineering and Geosciences, Delft University of Technology, Delft, the Netherlands
[3]Department of Geological Engineering, Faculty of Engineering, Hacettepe University, Beytepe, Ankara, Turkey

Received: 18.06.2012 • **Accepted:** 28.01.2013 • **Published Online:** 26.08.2013 • **Printed:** 25.09.2013

Abstract: We present a new 3D geologic model for the architecture and Cenozoic tectonic evolution of the Tuz Gölü Basin, a major sedimentary basin in the Central Anatolian orogenic plateau. This model is grounded on 7 depth-converted seismic reflection profiles in combination with the analysis of backstripped subsidence curves, isochore maps, and a palinspastically restored cross-section. Two stages of basin formation are detected during Cenozoic times. During the Palaeogene, around 2 km of basement subsidence led to the development of a sag basin broader than the present basin in the absence of bounding faults. After a period of uplift and erosion, sedimentation restarted by Tortonian times. Up to 3.5 km of post-Palaeogene sediments were deposited in relation to this second regional subsidence phase, which continued possibly well into the Pliocene. During this time, the 2 main fault systems found in the area, the Tuz Gölü and the Sultanhanı faults, developed as south-west dipping, NW–SE striking, normal faults. At some time in the Late Miocene-Early Pliocene, during regional subsidence, a previously unreported phase of contraction occurred, which led to the development of a north-east–vergent thrust sheet, the culmination of which forms the morphologic ridge to the east of the Tuz Gölü Lake. This structure presently divides the previously continuous Tuz Gölü Basin. Finally, minor extensional reactivation occurred. At the regional scale, the pre-Late Miocene subsidence is coeval with the initiation of volcanism in the Central Anatolian Volcanic Province and marine carbonate deposition in southern Turkey, and the latest Miocene shortening is (partly) contemporaneous with the onset of uplift in the same region.

Key words: Central Anatolian Plateau, Turkey, Tuz Gölü Lake, Cenozoic, Miocene, vertical tectonics, thrust

1. Introduction

Collision between the Eurasian and Arabian plates initiated orogenic build-up and crustal shortening in the Eastern Anatolian Plateau (e.g., Şengör & Yılmaz 1981; Dewey *et al.* 1986; Keskin 2003; Okay *et al.* 2010). To the west, the Neogene Central Anatolian Plateau (CAP), delineated by the Pontide and Tauride mountain ranges, has a less clear kinematic and geodynamic evolution due to the scarcity of structural data on the Miocene rocks.

Prior to the CAP formation, during the Late Cretaceous to Late Palaeocene, several continental blocks collided in Turkey (e.g., Şengör & Yılmaz 1981; Görür *et al.* 1984, 1998; Şengör *et al.* 1984; Williams *et al.* 1995; Robertson 1998; Hüsing *et al.* 2009) (Figure 1). This continental gathering caused regional uplift that led to fluvio-lacustrine deposition in the central domains (e.g., Görür *et al.* 1984), and initial formation of topography and rise above sea level in both the Pontides and the Taurides. This happened by Eocene times in the Pontides (e.g., Şengör & Yılmaz 1981; Şengör *et al.* 1984), as shown by nonmarine deposition and the absence of Upper Palaeogene rocks (e.g., Robinson *et al.* 1995; Rojay 1995), and by the Early Oligocene in the Taurides (e.g., Eriş *et al.* 2005; Jaffey & Robertson 2005), where continental deposition took place (e.g., Bassant *et al.* 2005; Şafak *et al.* 2005). Subsequently, a period of regional subsidence occurred, which initiated the deposition of marine sediments in the south and north of the plateau. Meanwhile, in Central Anatolia the continued deposition of continental sediments led to the formation of a system of Late Cenozoic or younger interior basins (Çemen *et al.* 1999). The end of the marine sedimentation in the southern margin of the CAP (Bassant *et al.* 2005; Çiner *et al.* 2008), probably marking the onset of the succeeding surface uplift event, has recently been dated by Cosentino *et al.* (2012) to be as young as ~8 Ma. Similarly, the surface uplift in the northern margin of the plateau has been reported to be Late Miocene-Early Pliocene (Yıldırım *et al.* 2011). However, these uplift events have not been linked to the centre of the system and the tectonic regime in the CAP interior during Miocene

* Correspondence: d.fernandezblanco@vu.nl

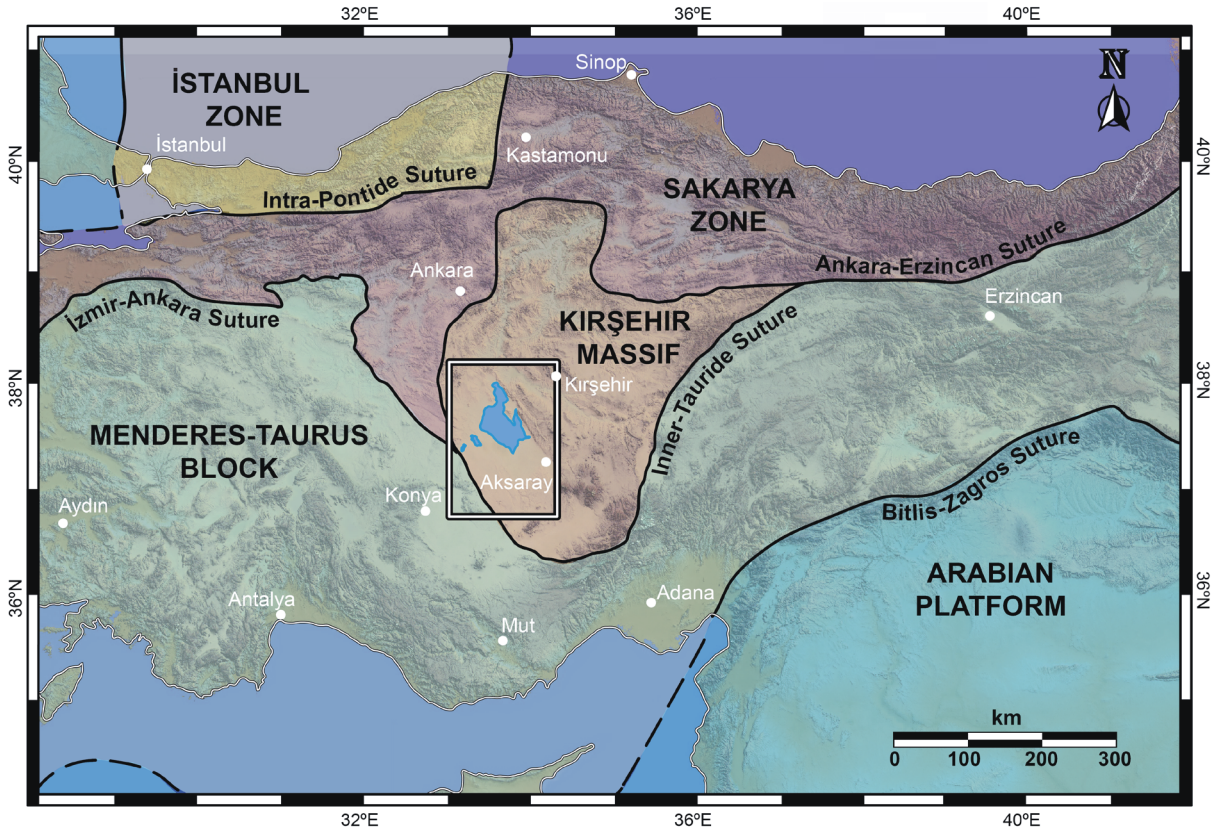

Figure 1. Palaeoterrain map of the area, showing the main tectonic elements of Turkey and the location of the study area. The slight modification of the location of the boundaries after Okay and Tüysüz (1999) is based on analysis of a set of 1 arc DEM and LandSat 7 images from NASA.

times is still under debate (see Genç & Yürür 2010 for a recent example). Understanding the structural pattern as well as an accurate timing of the main deformation events in the area will give relevant constraints on the mode and genetic nature of the CAP build-up and information on plateau genesis elsewhere.

Previous studies in Central Anatolia were centred on its pre-Miocene evolution (e.g., Uğurtaş 1975; Şengör & Yılmaz 1981; Görür *et al.* 1984). Early works mostly concentrated on sedimentological approaches (e.g., Arıkan 1975), whereas more recent studies used geophysical data (Gürbüz & Evans 1991; Aydemir & Ateş 2005, 2006a, 2006b, 2008; Önal *et al.* 2008). On the other hand, several studies have centred on the present tectonic regime and type of faulting (Dirik & Göncüoğlu 1996; Çemen *et al.* 1999; Özsayın & Dirik 2007; Çiner *et al.* 2011; Özsayın & Dirik 2011).

The Tuz Gölü Basin (TGB) is a major representative amongst the CAP interior basins (Dirik & Erol 2000). Here, we aim to reconstruct the Miocene structural evolution of the TGB and surrounding areas in relation to its regional context. For this, we have interpreted and converted to depth 7 seismic reflection profiles at eastern and southern locations with respect to Tuz Gölü Lake, analysing structures and sedimentary body geometries. On the basis of the geological sections, we have constructed the following for the Miocene units: (i) isochore maps to resolve their sedimentary distribution, (ii) backstripped subsidence curves to determine the vertical movements, and (iii) a palinspastically retrodeformed section to quantify the horizontal deformations. The horizontal motions were then compared with the vertical motions. The final output is a 3D evolutionary model of the tectonic movements undergone by the area since Palaeogene times.

2. Study area

The study area is located in central Turkey, at an average elevation of ~1.1 km, covering a relevant part of the TGB (s.l.) (as defined by Görür *et al.* 1984). A NW–SE trending relief called the Şereflikoçhisar–Aksaray Ridge (SAR) stands out of the remarkably flat topography of Tuz Gölü Lake and its surroundings (Figure 2). Presently, the central domain of the study area is mostly covered by unconformable Miocene or younger units, with the exception of an elongated area of Cretaceous and Palaeogene rocks that outcrop along the SAR (Figure 2).

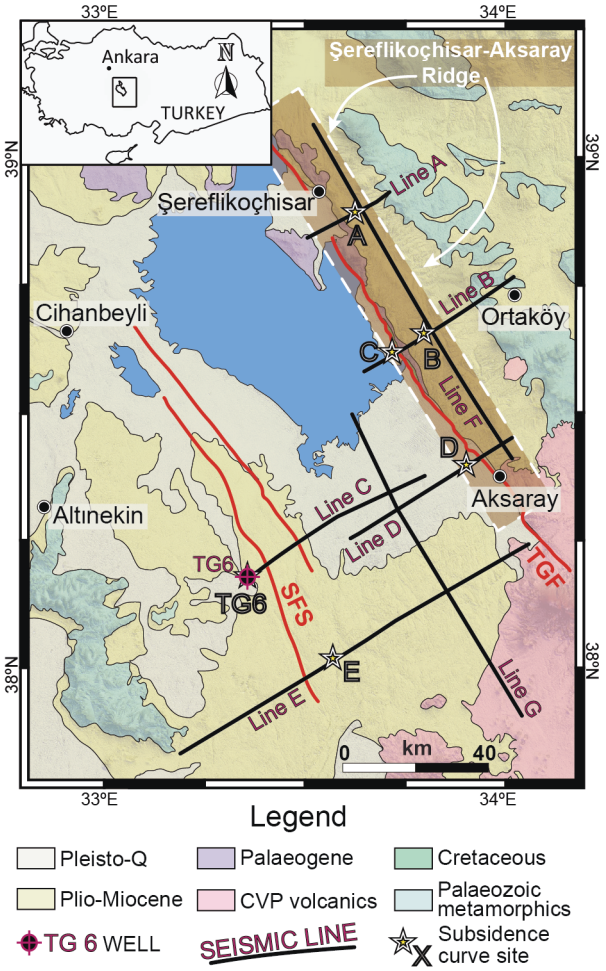

Figure 2. Tuz Gölü Basin geologic and data location map, depicting lithological distributions as in the geologic map from the General Directorate of Mineral Research and Exploration of Turkey (MTA). The locations of the 7 interpreted seismic reflection lines and the TG6 borehole are shown as well as the position of the sites chosen for subsidence analysis. The main fault systems are illustrated in red.

The SAR is bounded to the south-west by the Tuz Gölü Fault (TGF). Oriented parallel to the elongation of the high relief, the south-west dipping TGF represents one of the most important structures in Central Anatolia. This dextrally oblique normal fault (Dirik & Erol 2000; Huvaz 2009), together with the strike-slip Yeniceoba–Cihanbeyli Fault System in the west (Özsayın & Dirik 2007) and its southward continuation, the Sultanhanı Fault System (SFS), have been classically considered to be basin-forming structures (Figure 2).

3. Data and methods

The TG6 well and 7 seismic reflection profiles were selected for interpretation from the data set provided by the General Directorate of Petroleum Affairs (data

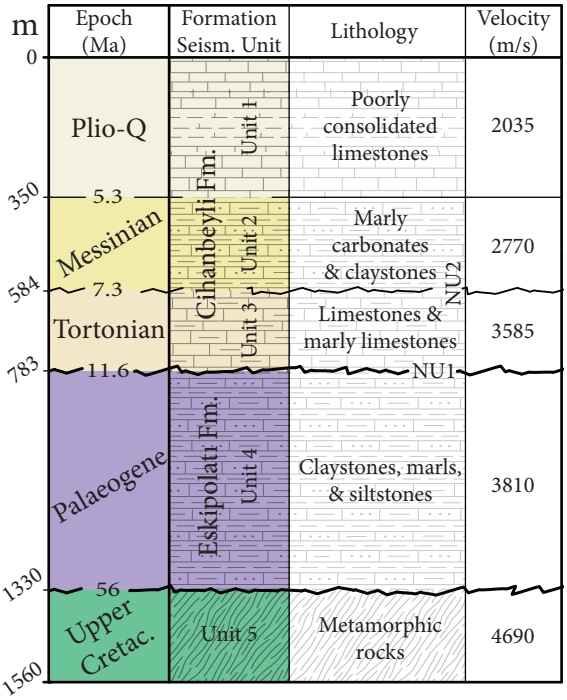

Figure 3. The TG6 well data and velocity model adopted for depth conversion. Within the Miocene package, different intervals are defined on the basis of strong lithological contrasts in conjunction with changes in the sonic log signal. Mean average interval velocities are obtained assuming constant velocities along each unit interval, and defined taking into account the slowness signal and the different fractions of lithology content of each unit.

set obtained by the Turkish Petroleum Corporation (TPAO) in its 1990 and 1991 campaigns). The lines are located around the present-day Tuz Gölü Lake; 5 of them are perpendicular to the SAR, while 2 are parallel to it (Figure 2). The NE–SW seismic lines transverse the main structures of the basin whereas the 2 parallel profiles image the basin in the NNW–SSE direction. The lines cover some 100 km in the north-east direction and ca. 150 km in the NNW direction, with a lateral separation between them of around 30 km in both directions. The seismic lines were originally supplied as .tiff images and were then converted to SegY format using GeoSuite AllWorks® and the original recording parameters. Analysis of the seismic signal and interpretation were done on the time section and then converted to depth on the basis of sonic log velocities from well TG6 (Figure 3).

3.1. Seismic units and facies

Unit 1, in the uppermost part of the seismic images, has no or very weak reflections, being mostly transparent due to a lack of signal in at least the first 200–400 m. Its base was chosen by means of lithological and seismic velocity characteristics observed in the TG6 well and extended along the rest of the lines (Figure 4).

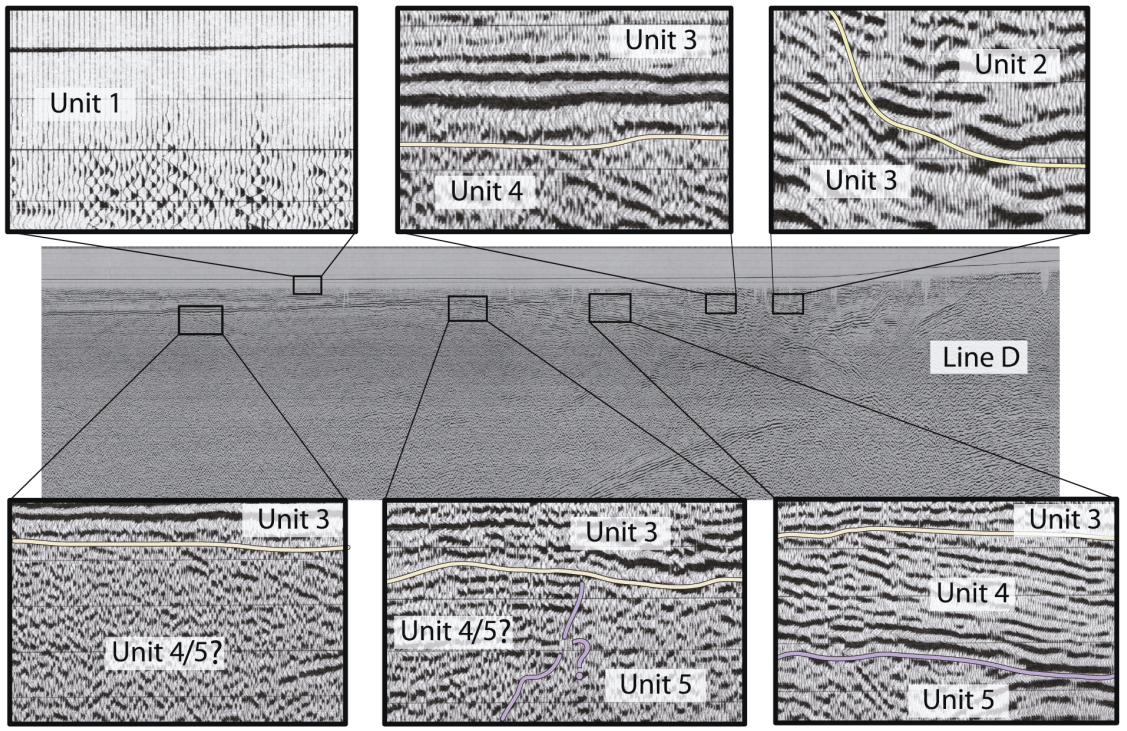

Figure 4. The main seismic facies identified for the seismic sections of the study area, shown on line D.

Unit 2 is a seismic package of continuous and rhythmic but often weak reflections. A low angle erosional unconformity marks the base boundary of Unit 2. This surface is a clear diagnostic feature of the seismic lines (Figure 4) and corresponds to the Neogene Unconformity 2 (NU2) of Uğurtaş (1975). However, the NU2 cannot be correlated throughout the study area as it becomes less angular in many locations.

Below the NU2, Unit 3 is a characteristic seismic package with continuous and generally high-frequency rhythmic reflections. The bottom of Unit 3 is formed by 2 very strong positive regional reflections followed by a low reflective area. The underlying angular unconformity marks the base of this unit. This regional surface, named Neogene Unconformity 1 (NU1) by Uğurtaş (1975), corresponds to the base of the Miocene deposits in the area and encompasses a hiatus of up to 17 My (Genç & Yürür 2010) (Figures 3 and 4).

Three different situations can be found for the distribution of units below the Miocene (Figure 4): (i) areas where Unit 3 is unconformably above the incoherent and/or irregularly distributed low-frequency reflections of Unit 5; (ii) areas where Unit 3 is above a package of midfrequency laterally discontinuous deformed reflections, named Unit 4, which is in turn unconformably deposited on top of Unit 5; and (iii) areas where the unclear nature of the reflections does not permit discrimination between units 4 and 5. Unit 4 generally corresponds to Palaeogene rocks. To the south-west of the study area, Unit 4 might instead correspond to evaporitic bodies, as stated in the study carried out by Uğurtaş (1975), who defined the presence of salt walls with closer-spaced, higher-definition seismic lines. Unit 5 represents the acoustic basement formed by metamorphic rocks.

3.2. Seismic-to-well tie and time-to-depth conversion

The seismic-to-well "tie" is a common technique used to associate geological units to the seismic units defined by seismic facies analysis, thus assigning geologic value to the seismic signal.

One single well (TG6) that contained a (partial) sonic log record was available for analysis (Figures 2 and 3). The TG6 well penetrates 1560 m of Eocene-Recent carbonates, marls, silts, and sands before it reaches the rocks of the Cretaceous ophiolitic mélange (Derman *et al.* 2000). The defined Quaternary to Cenozoic formations are described as Cihanbeyli and Eskipolatlı formations for the area, and the assigned ages at their bases are Tortonian and Eocene, respectively (Görür *et al.* 1984; Özkan Huvaz, 2012, personal communication). The Cihanbeyli formation (upper 783 m) is formed by limestones, marls, and clays (Figure 3). Three intervals were defined within the Cihanbeyli formation on the basis of interval velocity, lithological differences, and seismic facies characteristics. The basal interval correlates with the base of the Cihanbeyli formation, which is of Tortonian age (Özkan Huvaz, 2012, personal communication). The upper interval presents

typical interval velocities of unconsolidated sediments and is therefore assigned to be Pliocene in age. The intermediate interval shows distinctive seismic velocities, varying more than 500 m/s with respect to either the basal or the top intervals. This interval also shows a distinctive seismic facies character. Therefore, this interval is assumed to correspond to sediments of roughly Messinian age. Thus, the basal surface of these intervals/units roughly corresponds to Pliocene (Unit 1), Messinian (Unit 2), and Tortonian (Unit 3). The Eskipolatlı formation is enclosed between unconformities and comprises 547 m of clay, marls, and silts. This formation is Palaeogene in age and it is considered to correspond to Unit 4. Unit 5 is linked to Cretaceous rocks.

After the definition of these units, the TG6 well was linked to seismic line C, which passes through the well site. Since the seismic lines cross-cut each other (Figure 2), these newly defined horizons were used for correlation throughout the area by means of the seismic facies. This correlation was partly direct, continuing specific seismic facies units, and partly jump-correlated, where no direct connection amongst reflections was possible. The latter procedure was followed for the base of Unit 1 and for the contact between units 4 and 5, where differentiation between the units is often not clear.

In order to avoid time-related artefacts, the seismic lines presented here were converted to true depth using GeoSuite AllWorks® and the velocity values shown in Figure 3. The average interval velocities were obtained assuming constant slowness velocities in each depth interval and weighted lithological standard velocities (Bourbie *et al.* 1992). Among the available techniques, this method is geologically the most reliable, considering both the nonuniqueness associated with the construction of velocity models (Al-Chalabi 1997a, 1997b; Reilly 1993) and that Dix equations (Dix 1955) are only valid for homogeneous isotropic low-steepness layers. Although using standard velocity values extracted from the sonic log is a rough approach, it is appropriate for our purposes as no important variation in density or in compaction by overburden can be assumed. Furthermore, the obtained values (Figure 3) are consistent with those of Aydemir and Ateş (2006a, 2006b).

4. Seismic lines

4.1. NE–SW trending sections

4.1.1. Seismic line A

This seismic line is the northernmost section in the study area. Located near Tuz Gölü Lake, line A partly covers the small Şereflikoçhisar peninsula, crosses the SAR, and continues to the north-east (Figure 2).

The SAR separates line A in 2 different domains. At both sides of the SAR, 2 fault systems are seen, the TGF and a thrust linked to it, the Şereflikoçhisar–Aksaray Thrust (SAT), reported here for the first time (Figure 5).

These 2 prominent south-west dipping faults and a series of west- (but also east-) dipping faults constitute the Tuz Gölü Fault System (TGFS). Figure 5 shows that these faults cross-cut each other and some were reactivated, as happened for the TGF (s.s.). This is seen in the western side of the fault system as a rollover anticline and a harpoon-shaped inversion geometry. Other fault structures to the north-east of the TGFS depict minor horst shapes for the lower part of Unit 3. To the south-west of the TGFS, several normal faults offset all the Cenozoic sequences.

A 3-km-wide thickened area affected by diffuse extensional features is seen immediately to the south-west of the SAR, while to the north-east, the units are thickening toward it progressively. Unit 1 has maximum thicknesses of 250 m in the thickened area south-west of the TGF, and thins south-westward in a horizontal space of 5 km. On the other hand, nearly constant thicknesses of less than 100 m are seen for this unit in the north-eastern side of the SAT. Unit 2 wedges in toward the SAR and reaches its maximum thickness, ~600 m, near the SAT. On the western side of the SAR, near the TGF, Unit 2 is 2 times thinner. Elsewhere along line A, Unit 2 has thicknesses of some 50–200 m. In a similar fashion as Unit 2, the distribution of Unit 3 shows relevant thickening toward the TGF and the SAT. The Unit 3 thickening is related to normal faults in the south-western thickened area, and is twice as thick in the north-eastern side of these structures. Unit 3 has average thicknesses of ~100–400 m and maximum thicknesses of some 1200 m in the north-east part of the SAT. The contact between units 3 and 4 is apparent in the south-western side of the TGF, with reflections marking an angular unconformity. The thickened structure seen south-west of the TGF for these units is not repeated in Unit 4. Instead, a prominent south-westward–thickening wedge is seen along the entire profile. For Unit 4, the thickening of sediments occurs from the north-east to the south-west, from ±750 m to ±2800 m, and its base deepens from 1 km to 3 km in the same direction. Neither the Miocene units (units 1 to 3) nor the Palaeogene unit (Unit 4) have reflections that indicate basin terminations.

4.1.2. Seismic line B

Seismic line B lies around 30 km to the SE of line A (Figure 2). Similar to the line described above, this line crosses the TGF and the SAR. Even though sediment distribution and fault morphologies resemble those found in line A, some important differences are observed.

Three major extensional systems on the sides of the SAR are seen in line B (Figure 5). These faults are the described south-west dipping TGF and SAT and a major deep-rooted normal fault dipping north-east. Together they form a horst that is mimicked by several smaller faults offsetting units 2 to 5. A well-developed rollover anticline with a harpoon structure is seen on the south-western

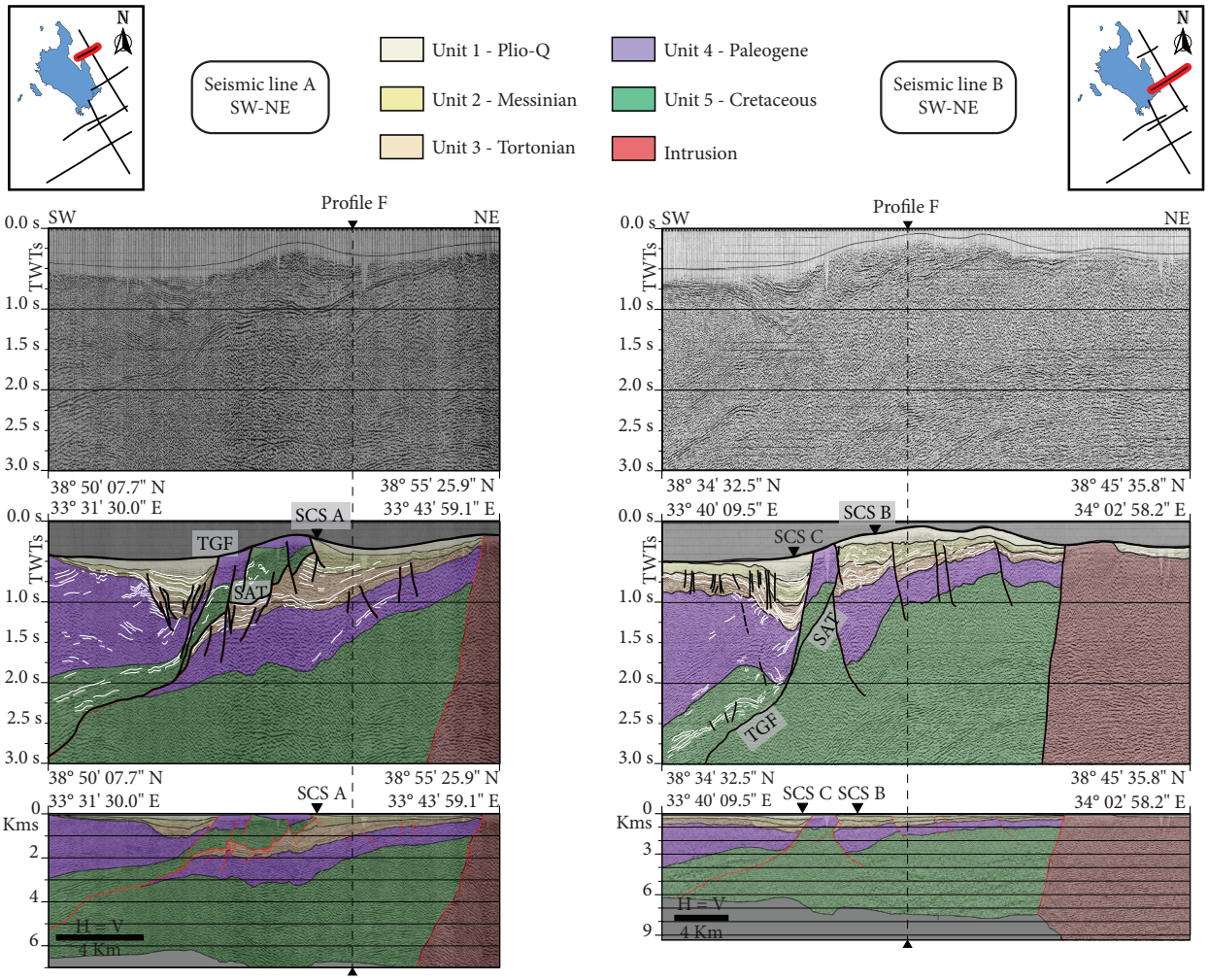

Figure 5. Northern NE–SW oriented lines. The original seismic image, seismic interpretation in 2-way time (TWT), and depth-converted profile for lines A and B. The location map and intersection with other seismic profiles used in this study are also shown.

side of the TGF. Other minor normal faults are observed, especially on the south-western side of the line.

Thickening of the Neogene package (units 1, 2, and 3) occurs toward the 3 major faults. These units have no basin-termination reflections on either side of the line. Close to the TGF to the south-west, Unit 1 shows a thickened area of about 400 m that thins toward the west from approximately 4.5 km of thickness to less than 50 m. To the north-east of the SAT, Unit 1 shows an approximately 15-km-wide shallow depression with a maximum thickness of around 250 m in its middle part. Deepening in the section, Unit 2 depicts similar thickness distributions as Unit 1. The thicknesses of Unit 2 are 1.5 times larger on the north-eastern side of the TGF with respect its south-western side. The thickened area is again seen on the western side of the TGF, although thinning toward the south-west is not evident. Unit 2 maintains relatively constant thicknesses toward the south-west (around 200–250 m), but thins away from these fault systems on the north-eastern side. In a similar manner, Unit 3 thickens toward the TGF and the SAT. To the south-west of the TGF, Unit 3 thicknesses reach some 700 m. Constant thicknesses of around 450–500 m are maintained for this unit toward the south-west. The shallowing of the base of Unit 3 while moving south-west away from the TGF ends within 3 km, where its base becomes horizontal. To the north-east, close to the SAT, Unit 3 thicknesses are ±650 m. Unit 3 thins toward the north-east to around 200–250 m on the north-eastern–most part of the line. Wedging toward the south-west of Unit 4 is another remarkable feature, with thicknesses ranging from ca. 500 m on the north-east of the line to ±3000 m on the south-west of it, where the base of Unit 4 deepens to ca. 3700 m.

4.1.3. Seismic lines C and D

Seismic sections C and D lie some 35 km SE of line B (Figure 6). These SW–NE oriented lines are shifted approximately

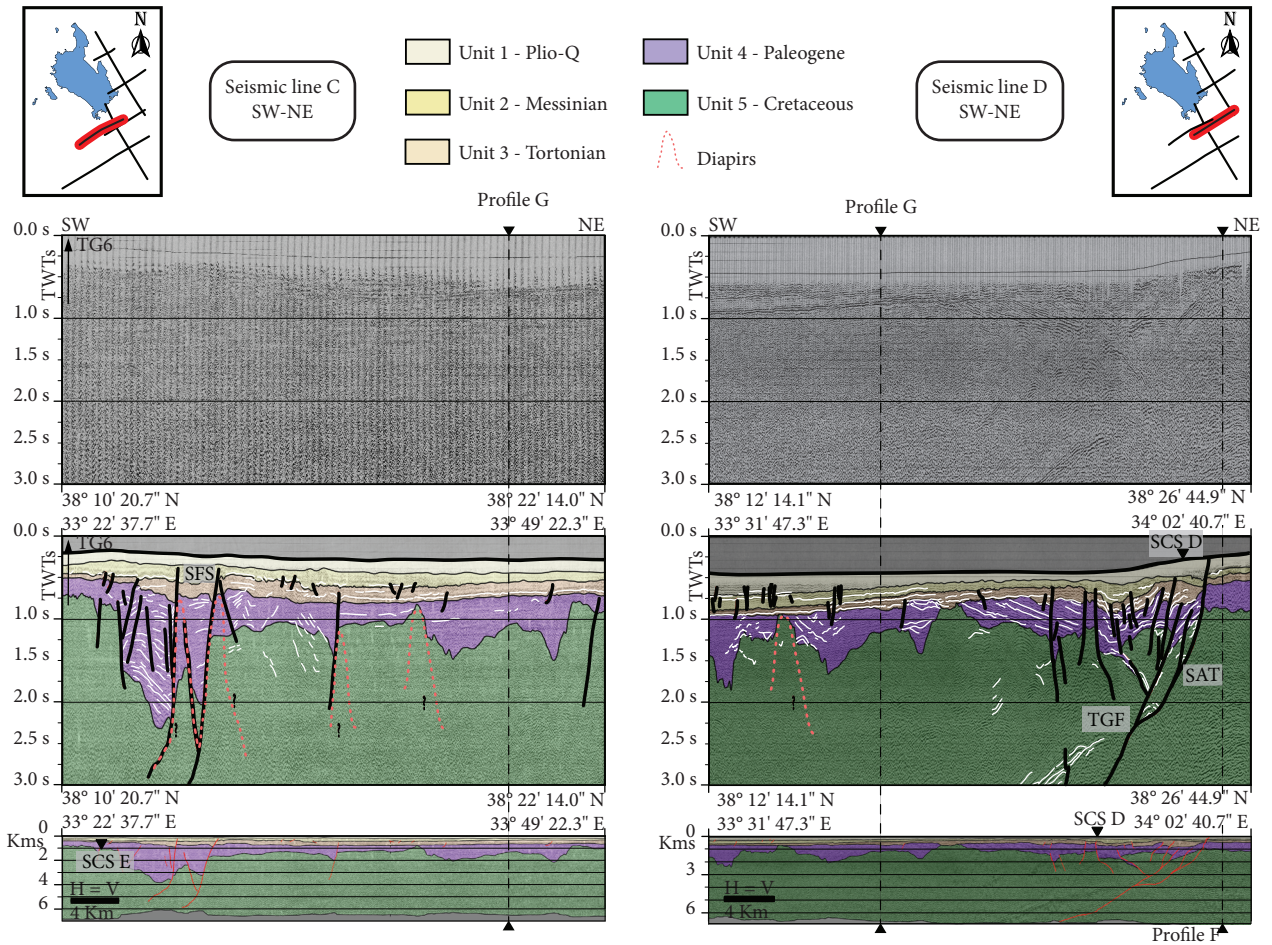

Figure 6. Centre NE–SW oriented lines. The original seismic image, seismic interpretation in TWT, and depth-converted profile for lines C and D. The location map and intersection with other seismic profiles used in this study are also shown.

5 km in the NW–SE direction (Figure 2), with the north-eastern sector of line C and the south-western sector of line D depicting the same geologic features. Therefore, these lines have been analysed together. The north-eastern side of line D ends inside the SAR, thus providing no information about the basin on that side of the high. The base of the Neogene units shows relatively constant depths, with 2 maxima associated with the main fault systems, the SFS in the west and the TGF in the east (Figure 6). The SFS is seen as 2 prominent south-west–dipping faults (profile C in Figure 6) offsetting Unit 3, the middle part of Unit 2 of the Neogene package (approximately Upper Miocene), and several associated structures. In a similar manner, the TGF is a south-west dipping feature with several associated faults (profile D in Figure 6). These faults show extensional as well as contractional features, but the harpoon structure is not well defined. Considering its location, the easternmost fault of the line could be the SAT; however, the lack of reverse offset points to it being an extensional fault part of the TGFS. Extensional secondary faults also accommodate the movement in the western side of the TGF.

Thickening of units 1, 2, and 3 to the north-east of the TGF is not seen. The Neogene units depict limited thicknesses on that side of the fault and the depth at their base is less than 500 m. Within the Neogene package, Unit 1 has a fairy continuous thickness with a maximum of 200 m. The thicknesses of Unit 2 are around 300–400 m and fairly continuous. The thicknesses of Unit 3 range from some 400 m to 600 m. When affected by the major structures, Unit 3 has maximum thicknesses of ±1000 m. The angular unconformity between Unit 3 and Unit 4 is clearly revealed in both profiles. The Unit 4 reflections are irregularly deformed and show high dip angles (better seen in profile D). The bottom of Unit 4 seems to be deposited on an inherited palaeotopography and shows large variations in depth (from less than 1 km to about 4 km). The combined action of salt diapirs in this area (Uğurtaş 1975) and movements along the faults of the SFS might have caused the morphology observed in the south-

west part of profile C. Thicknesses of more than 3 km can be seen for Unit 4 in relation to the SFS.

4.1.4. Seismic line E

Seismic profile E is located some 30 km south-east of line D (Figure 2). The north-east end of line E ends close to the TGF, while the SFS can be seen at its south-west end (Figure 7).

The most apparent structure seen in line E is the SFS, situated around the centre of this line. The SFS is composed of 2 major south-west dipping extensional faults reaching the base of Unit 2 and at least 2 similar but relatively minor structures toward the north-east. Numerous other secondary normal structures were found between the SFS and the north-eastern end of the section (Figure 7). Units 1, 2, and 3 thicken when affected by the SFS and the other analogous structures. This thickening is seen for units 1 and 2 and reaches values of around 500 m for Unit 3. Unit 4 also shows thickening caused by the SFS. Toward the north-east end of the line, the thickening of Unit 4 indicates a proximity to the west side of the TGF.

4.2. NNW–SSE trending sections

Lines F and G are oriented parallel to one another and shifted laterally ~35 km. The southernmost area of line F and the northernmost area of line G are coincidental and depict similar geologic features for ~35 km. When both lines are taken together, they result in an approximately 170-km-long section across the TGB parallel to the SAR. These lines share similar patterns and thicknesses of the seismic units and depict the same structures. Thus, they are described here together (Figures 8 and 9).

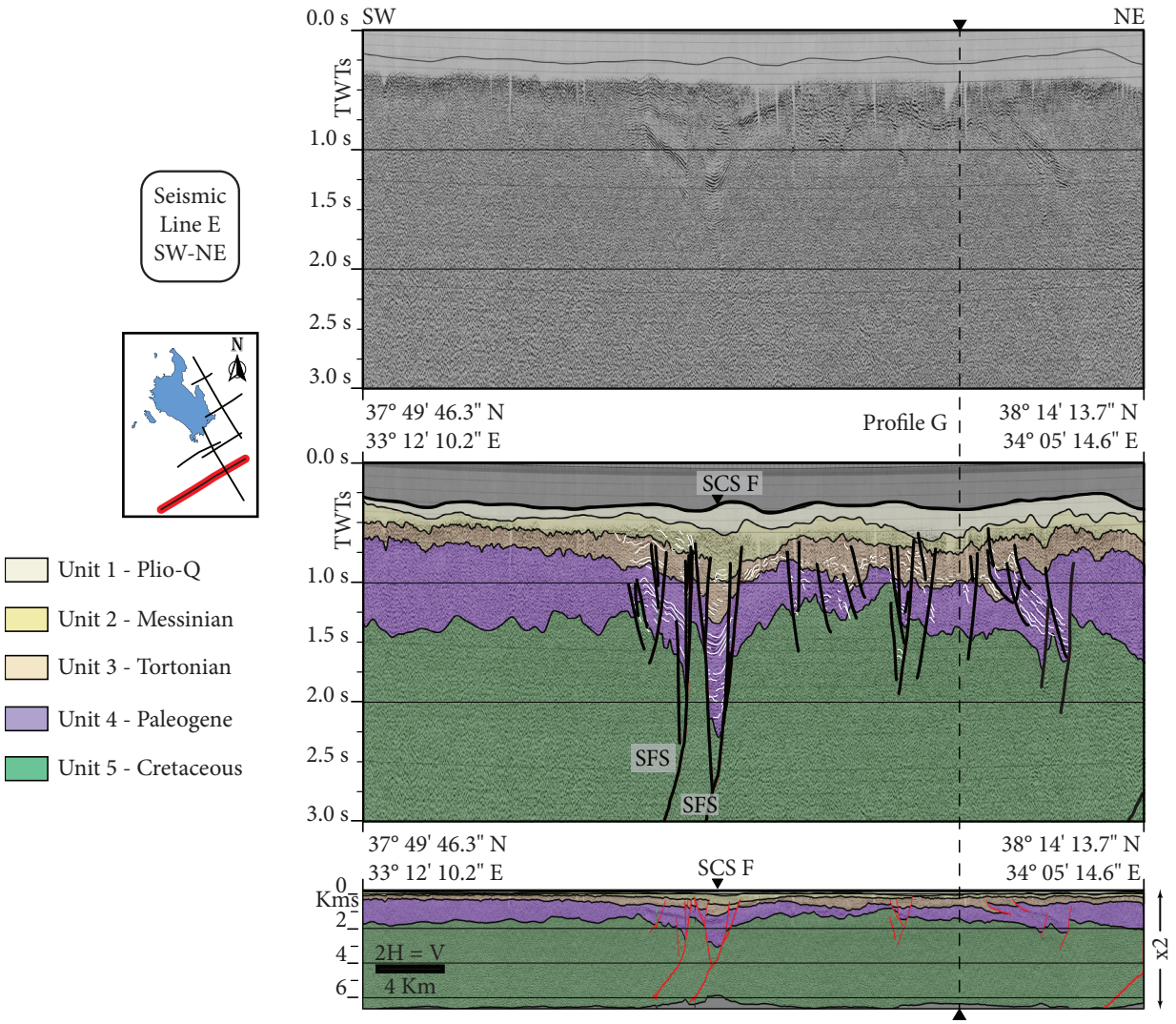

Figure 7. Southern NE–SW oriented line. The original seismic image, seismic interpretation in TWT, and depth-converted profile for line E. The location map and intersection with other seismic profiles used in this study are also shown. The longest seismic profile is in the NE–SW direction (±120 km), and so this is represented with double vertical exaggeration.

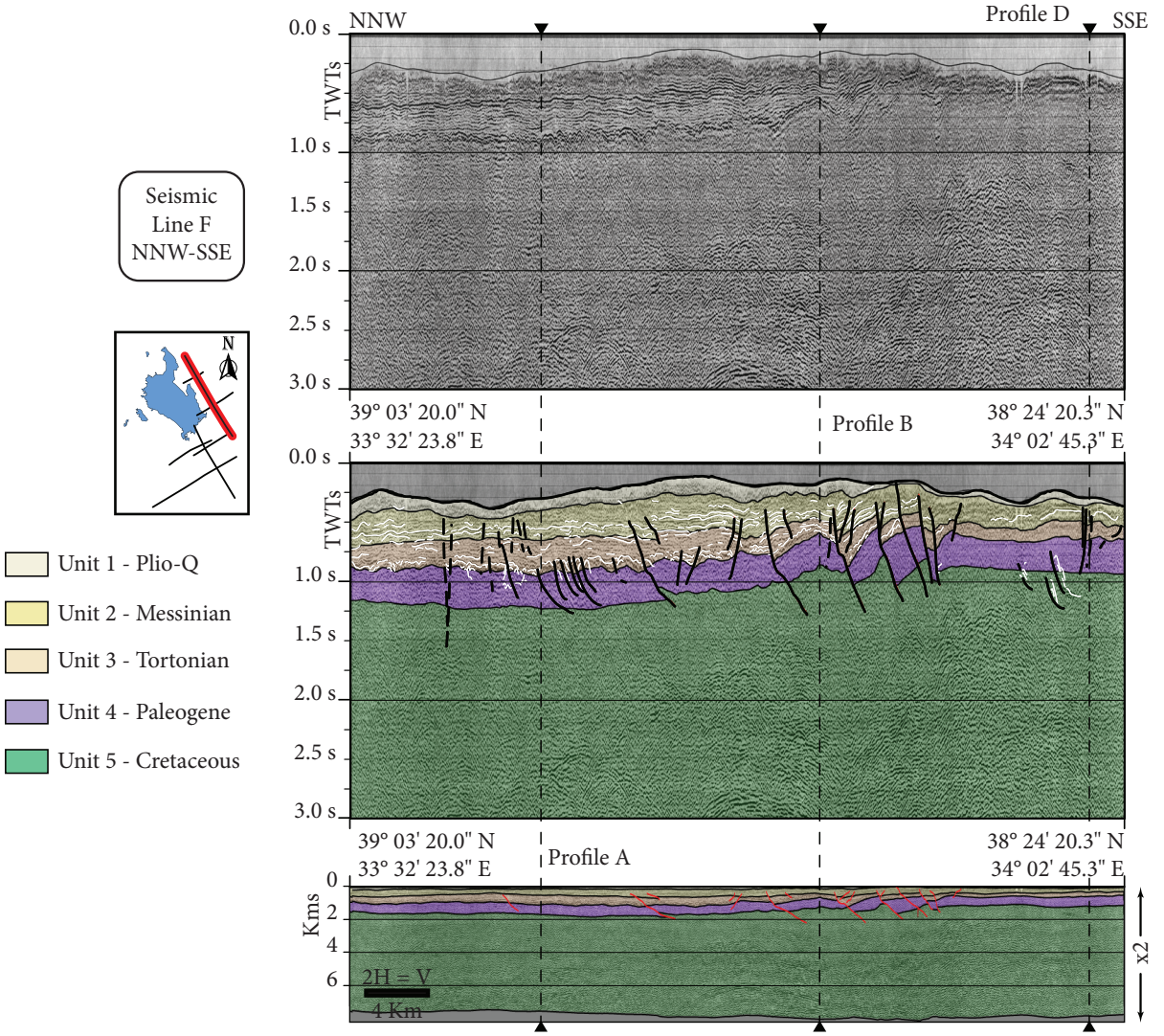

Figure 8. Eastern NNW–SSE oriented line. The original seismic image, seismic interpretation in TWT, and depth-converted profile for line F. The location map and intersection with other seismic profiles used in this study are also shown. The line is shown with double vertical exaggeration.

The thicknesses of the seismic units in profiles F and G are fairly constant. The reflections show no basin terminations within the extent of the lines. However, variations in the trend of these units can be seen in both profiles. In line F, units 1, 2, and 3 thicken gently toward the NNW (Figure 8). The base of Unit 4 in line F deepens toward the north from 1 to 1.5 km and is offset by several normal faults, especially in the middle to southern parts of the profile. Most faults dip south and have vertical displacements up to 500 m. Line G shows thickening for Unit 2, and especially for Unit 3, towards the SSE (Figure 9). This western profile shows 1500–1700 m of continuous fairly horizontal depth for the base of Unit 4 and almost no disruption by faults.

5. Three-dimensional architecture of the TGB

As observed in the lines, the TGB presents small thickness variations for the main units in the NNW–SSE direction and more prominent ones in the NE–SW direction. In the NE–SW direction, the reflections in the upper section (uppermost 2 s) pinch out both north-eastward and south-westward from the TGF and the SAT, but no clear basin terminations can be seen on either side. Moreover, the pinching-out geometry is seen for the northern area but not in the southern part.

5.1. Composite section

A composite section has been constructed in the NE–SW direction in order to represent the overall sedimentary geometries and deformation structures (Figure 10). As

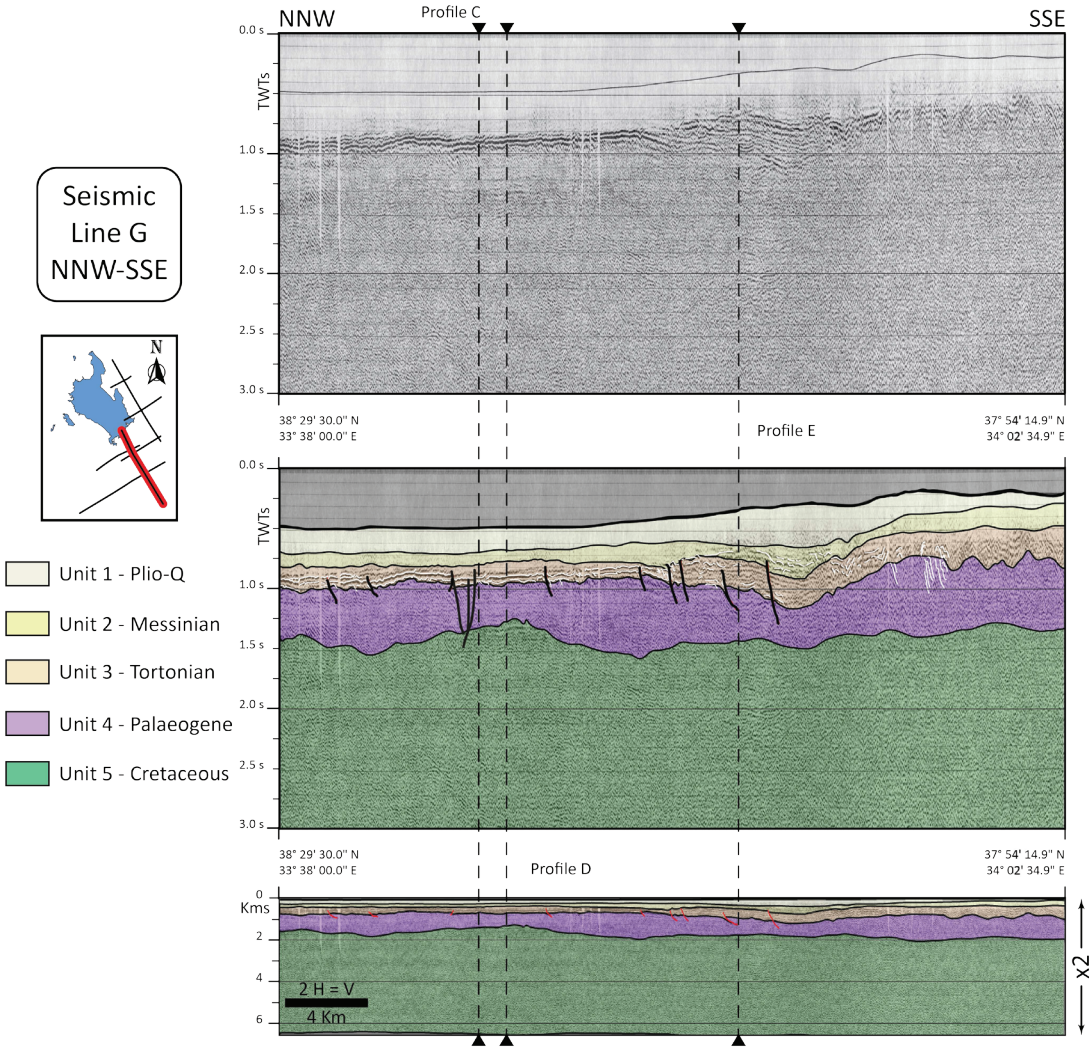

Figure 9. Western NNW–SSE oriented line. The original seismic image, seismic interpretation in TWT, and depth-converted profile for line G. The location map and intersection with other seismic profiles used in this study are also shown. The line is shown with double vertical exaggeration.

observed in this composite section, all the seismic units are continuous and the only disruption is in correspondence with the SAR, the SFS, and associated faults (Figure 10). The Plio-Quaternary unit (Unit 1) thickens in 3 different areas, the SFS, the TGFS, and in relation to a secondary fault system in the centre-left of the composite section. In contrast, units 2 and 3 show only 2 main depocentres. Units 2 and 3 are thickest in correspondence with the western side of the SFS and the TGFS, showing wedges at their western and eastern sides (Figure 10). The position of the base of Unit 4 has important variations, from less than 200 m to some 4 km in depth. Starting in the north-eastern part of the study area (Figures 2 and 10), Unit 4 shows growing thicknesses south-westward, with a maximum of ~3 km. This thickening is disrupted when moving toward the south-west along the composite section by either a palaeohigh or, more probably, a salt diapir. Unit 4 thins in this area to values of 500–800 m, remains fairly continuous in the south-western–most area, and thickens again to approximately 2.5 km in the SFS. The seismic units are continuous and the reflections show no basin terminations along the composite section.

Several secondary structures accommodated the movement imposed by these systems, thereby having analogous sediment relationships and orientations but smaller offsets. Other minor contractional as well as extensional faults affected units 2, 3, and 4, indicating a variety of events. The only seismic-scale folds seen are exclusively associated with fault movements.

5.2. The Şereflikoçhisar–Aksaray Ridge

The relief of the SAR, up to 250 m in variation, is the morphologic expression of the structures found

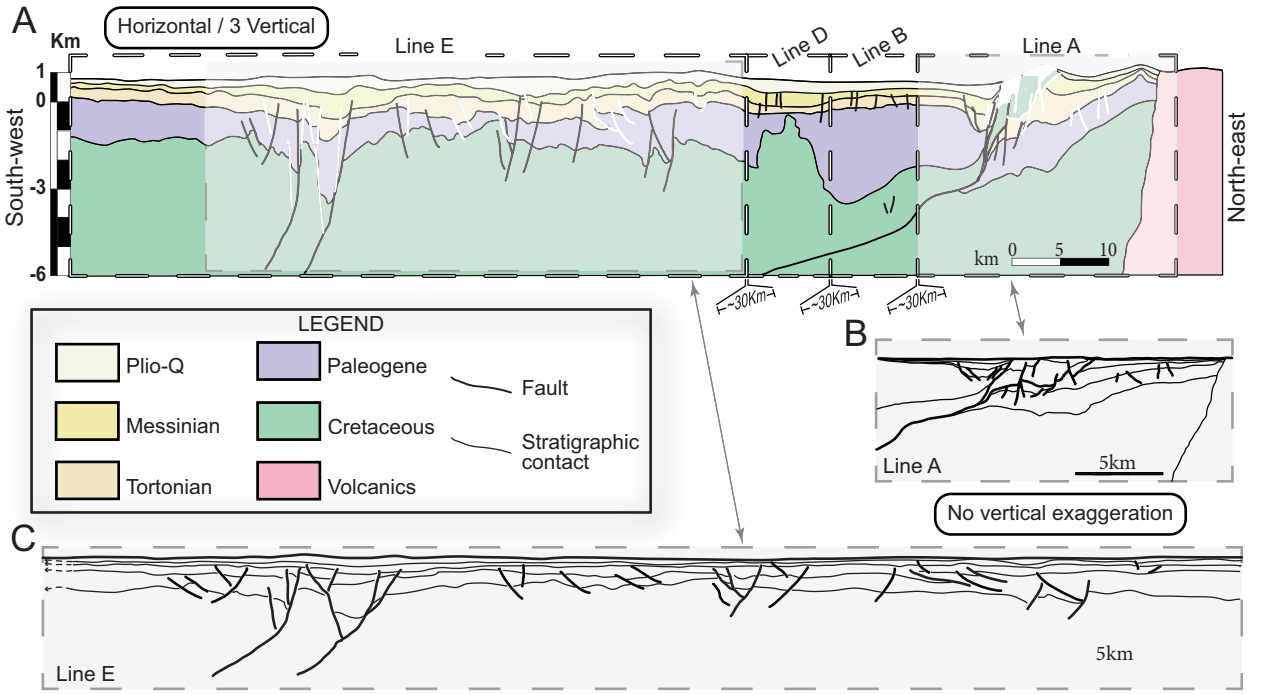

Figure 10. (A) Composite cross-section showing the main structures found in the study area, transecting them perpendicular to their main trends (SW–NE). This composite section is formed by 4 different seismic sections (from south-west to north-east, line E, line D, line B, and line A) that are separated by around 30 km from one another in the NNW–SSE direction. This profile is exaggerated 3 times in the vertical. (B & C) Depth-converted (scale 1:1) seismic interpretation of line A (used as input for the restoration and balancing) and line E.

underneath it, as observed in the seismic images. Under the SAR, the TGFS is a compound of 4 different fault families. There are 2 deep-rooted normal faults with opposite dips that create the main horst morphology. The TGF, which bounds the SAR to the south-west, is one of these faults. The SAT, linked with the TGF at depth, is a top to the north-east thrust outcropping Palaeogene and Cretaceous rocks in the core of the SAR and bounding it to the north-east. We also observe a series of extensional faults in the hanging wall of the TGF, thickening the Miocene sequence, and a second set of normal faults on the north-east side of the system, which are parallel to the primary structures and cut the thrust sheet. The cutting relationships amongst these fault families show 3 deformation phases. The older TGF extensional system is transected by the SAT, which is in turn cut by a younger stratigraphically higher system of normal faults. This clearly indicates a sequence of extension–shortening–extension events.

5.3. Sultanhanı Fault System

The major structures found in the SFS (Figure 10) are 2 normal south-west dipping faults involving basement. These 2 faults double the thicknesses of the Palaeogene unit and affect both Unit 2 and Unit 3. It was observed that the SFS is sealed by the upper part of Unit 2. The displacement and geometry of the different rock units offset by the SFS indicate an initiation of the system by Late Cretaceous times. On the eastern side, several mimicking structures closely resemble the morphology of the SFS, affecting the upper and lower boundaries of the Palaeogene unit. The fault system behaved as a right lateral transtensional fault zone in the Miocene and as a normal fault in the Pleistocene (Özsayın & Dirik 2011).

5.4. Structural map

Integrating literature data (Dirik & Erol 2000; Özsayın & Dirik 2007 and the references therein) with new observations found in the seismic lines and an analysis of 1 arc digital elevation model (DEM) and LandSat 7 images, an updated structural map was constructed for the study area (Figure 11). A NW–SE orientation of the major structures is clearly seen in this structural map. Most of the structures found in the area are extensional in character, with the exception of the SAT. The 2 main fault systems, the TGFS and the SFS, are laterally continuous structures. As observed in the structural map, the TGF and SAT components of the TGFS diverge north of Aksaray, limiting the Palaeogene and Cretaceous rocks to a narrow elongated area. The north continuation of the SFS widens into the İnönü-Eskişehir Fault System (Özsayın & Dirik 2007).

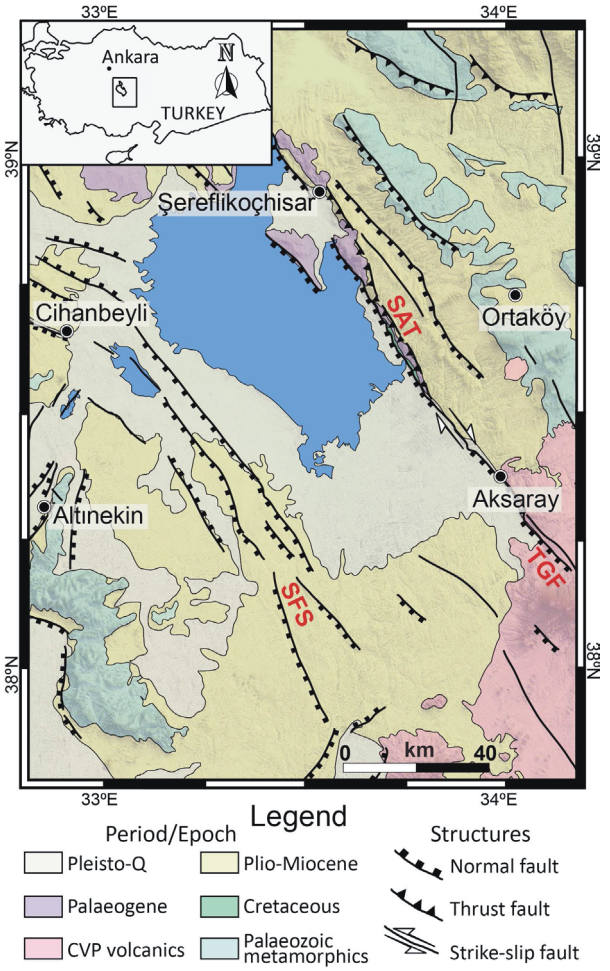

Figure 11. New structural map of the study area. Corrections to the locations of several structures and to the sense of movement were made on the basis of the analysis of the interpreted seismic refraction lines and a set of 1 arc DEM and LandSat 7 images from NASA. Modified after maps by Dirik and Erol (2000) and Özsayın and Dirik (2007).

5.5. Isochore maps

In order to understand the sediment accumulation patterns and the thickness distributions of the area, 2 isochore maps were made for units 2 and 3 representing the vertical sedimentary thicknesses. Isochore maps are constructed by subtracting the upper and lower boundary surfaces of each unit. Therefore, the isochore maps represent equal true vertical thicknesses of the unit, and are coincident with isopach maps only in horizontal layers. Precision of the thickness estimation depends primarily on the confidence of the seismic correlation of the base and the top of the target unit, which is variable but at a maximum for units 2 and 3. Another factor influencing the accuracy of the isochore maps is the extrapolation method used (kriging). The effects produced by the extrapolation were partially corrected by using a specified anisotropy of 325° N, i.e. giving a higher statistical load to values oriented parallel to the elongated trending of the basin, and by manual reinterpretation and correction of artefacts. Both maps show the present-day disposition of the sediments, without accounting for the distortions created by the main structures in the area (Figure 12).

The Unit 2 thickness accumulations show 2 different depocentres (Figure 12A), both NW–SE oriented, in the north-east and in the south-west. The north-eastern depocentre is divided in turn into 2 depressions on both sides of a NW–SE relative high, which corresponds to the SAR. Sediments to the west of this high cover a narrower area and are thinner than those lying in the eastern counterpart area. The presence of the TGF and the SAT might have been important by this time period, as seen by the development of the 2 differentiated depressions. The second depocentre, in the south-west, is broader than the former. In Unit 2, the sediment vertical thicknesses are at a maximum in this depocentre and reach some 500 m.

The isochore map for Unit 3 (Figure 12B) depicts 2 areas of strong accumulation (reaching 800 m and >900 m). Separated by a relative positive oriented NE–SW, these areas are striking broadly in the NW–SE and NE–SW directions, respectively. The northernmost depocentre is elongated and in alignment with the structural high seen for Unit 2. The south-western depocentre is shallower and broader than the northern depocentre. This area of low sediment accumulations might be a consequence of an inherited structural high located approximately parallel to the southern depocentre and might have forced NE–SW orientated deposition in it. This broad area of deposition is also affected by minor highs.

Comparison of these maps shows wider trenches of sedimentary accumulation for Unit 2 and narrower ones for Unit 3. The distribution of thicknesses seen for Unit 2 sediments, i.e. the differentiation of areas with small thickness accumulations that do not coincide with analogous features observed for younger times, indicates the probable presence of pre-Tortonian topography.

6. Tectonic motions in the Tuz Gölü Basin

6.1. Vertical movements

6.1.1. Methodology and data

We created 6 backstripped subsidence history plots for 6 localities corresponding to 5 synthetic wells obtained from the depth-converted sections, called subsistence curve sites (SCSs) A to E, and to the Tuz Gölü 6 well (SCS TG6) (Table 1). The sites were chosen in areas where the reliability of the seismic horizons was at a maximum and meaningful sediment thicknesses were found (Figure 2).

To produce the subsidence curves, information on absolute sea level fluctuations and palaeobathymetry is needed and the measured thicknesses need to be

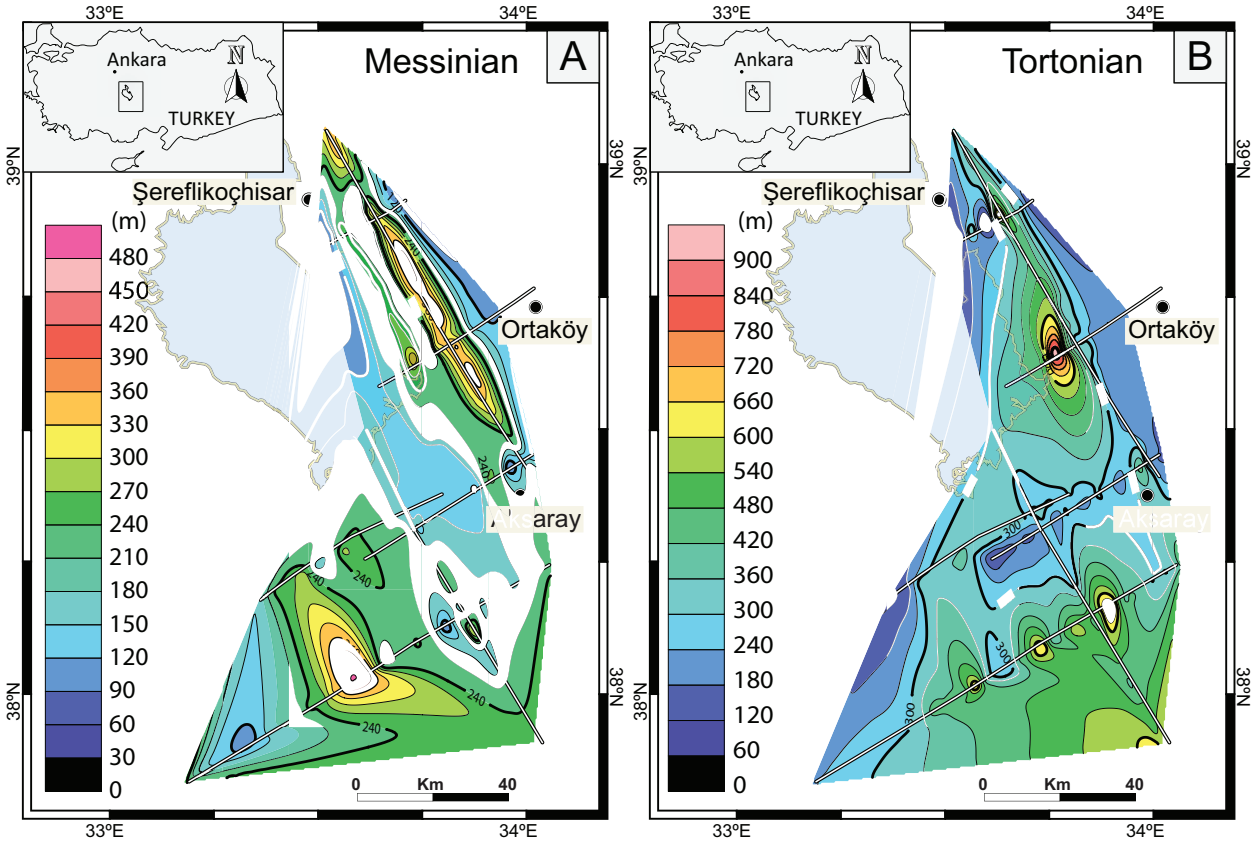

Figure 12. Isochore maps showing the thicknesses distribution of Unit 2 – Messinian (A) and Unit 3 – Tortonian (B). The thickness is represented in metres to the left of each figure. The locations of the seismic lines are also shown.

decompacted. Since the vast majority of the Tertiary to Quaternary sediments in the area are lacustrine to fluvial and palaeoaltitude information was not available, water depths were considered to be zero and do not necessarily correspond to sea level. Total decompacted thicknesses were calculated applying the approach of Steckler and Watts (1978), using standard mean, maximum, and minimum porosity–depth functions (Sclater & Christie 1980; Bond & Kominz 1984; Bessis 1986; Mavko *et al.* 2003). In order to correct for compaction, simplified lithologies have been assigned to each defined unit (Table 2), allowing for the definition of porosity and density as a function of depth. Proceeding in this manner, one-by-one decompaction of each package was subsequently produced along the minimum and the maximum porosity–depth curves. To construct the tectonic subsidence, the density of the entire sedimentary column was calculated and the depth of the basement was corrected for the sediment load assuming Airy isostasy and a mantle density of 3.3 g/cm^3.

We have limited our analysis to the time interval of the Tortonian to the present. The later upward movement shown in the plots is the result of adding the present-day

Table 1. Compacted thicknesses as measured on the synthetic wells and TG6 well.

Sites	Seismic unit thicknesses (m)			Elevation above sea level (m)
	Unit 1	Unit 2	Unit 3	
SCS A	120	330	550	1030
SCS B	150	350	500	1175
SCS C	375	425	480	900
SCS D	150	200	200	930
SCS TG6	340	244	199	1000
SCS E	170	450	620	1050

Table 2. Standard porosity–depth relationships.

0.29	0.216	0.4	0.51	1.0	Sand	Maximum porosity curve data
0.42	0.375	0.6	1.0	0.5	Silt	
0.5	0.475	0.7	1.1	0.5	Shale	
0.52	0.442	0.79	1.33	0.5	Carbonate	
0.0	0.1	0.0	0.1	0.0	Halite	
0.0	0.1	0.0	0.1	0.0	Anhydrite	
0.20	0.48	0.2	0.48	0.0	Sand	Minimum porosity curve data
0.25	0.325	0.25	0.325	0.0	Silt	
0.37	0.47	0.53	1.05	0.5	Shale	
0.20	0.58	0.2	0.58	0.0	Carbonate	
0.0	0.1	0.0	0.1	0.0	Halite	
0.0	0.1	0.0	0.1	0.0	Anhydrite	
φ_1	c_1 (km)	φ_0	c_0 (km)	z_p (km)	Lithology	

topography to the curve and has no tectonic meaning (Figure 13). To further understand the role of absolute elevations during basin development, we have investigated different scenarios.

6.1.2. Analysis of vertical motion

All subsidence plots (Figure 13) show continuous subsidence for the Late Miocene and part of the Pliocene, with fairly constant basement subsidence rates. Relatively similar trends are depicted for all the SCSs, i.e. subsidence rates are more pronounced during Miocene times and decrease during the early Pliocene (Figure 13).

However, some small differences amongst the chosen sites can be observed. SCS C, in the hanging wall of TGF, shows a high and almost continuous subsidence rate throughout all of the Miocene and the Early Pliocene (0.14 mm/year for both periods). Contrarily, the other site located in the TGF hanging wall, SCS D, shows continuous low rates (0.064 mm/year). SCS A and B, in the footwall of TGF, show intermediate values for the Miocene that decrease in Pliocene times (as low as 0.044 mm/year for SCS A). SCS E, located in the hanging wall of SFS, shows the highest rates (0.17 mm/year) during Miocene times, which decrease considerably during the Early Pliocene. In contrast, in the SFS footwall, the SCS TG6 shows low rates of basement subsidence in the Miocene and the highest subsidence rates (0.063 mm/year) in the Early Pliocene times.

The primary subsidence signals observed for all the subsidence curves indicate continuous regional subsidence in the area during Tortonian-Early Pliocene times. A relevant initial subsidence period took place in Tortonian or earlier times. During this initial phase, a NE–SW elongated area, comprising SCS D and SCS TG6, remained at a higher position. Subsequent lower subsidence rates occurred in Early Pliocene times. The relevant subsidence rates seen for both periods in SCS C might be associated with continued activity of the TGF. It is worth mentioning that both sides of the TGFS (NE–SW direction) show similar subsidence curves (see SCS A and SCS B) but relevant differences are seen between the northern (SCS A, B, and C) and southern sites (SCS D) along the strike of this system.

6.1.3. Scenarios of absolute elevation

The values of subsidence depths obtained for the reference scenario SCS C, discussed above, were compared with 2 different palaeoelevation scenarios to consider the influence of the palaeotopography (Figure 14). Scenario 1 assumes that a palaeoelevation equal to present-day topography (which we considered to be ~1 km) has existed since Tortonian times. In scenario 2, the palaeoelevation gradually grows from 0 km in Tortonian times, when subsidence was initiated, to 1 km at present times.

In scenario 1, the central panel (SCS C) reaches sea level depths by Late Miocene and Pliocene times. This signal is an indication that the sediment accumulation accounted for in the study area is unlikely to result from palaeotopography infill and may rather be a consequence of tectonic-driven subsidence. However, in this scenario, SCS D and SCS TG6 would have remained above sea level. This implies that SCS C and SCS TG6 were probably parts of elevated terrains (presently coinciding with the areas of the TGF and the SFS) while overall tectonic subsidence occurred in the area.

In scenario 2, the right panel (the tectonic basement curves) remains at sea level during the subsidence period due to the effect of the progressive uplift. The basement curve remains constantly under the sea level, and it reaches values of some 500 m by the Pliocene. The subsidence

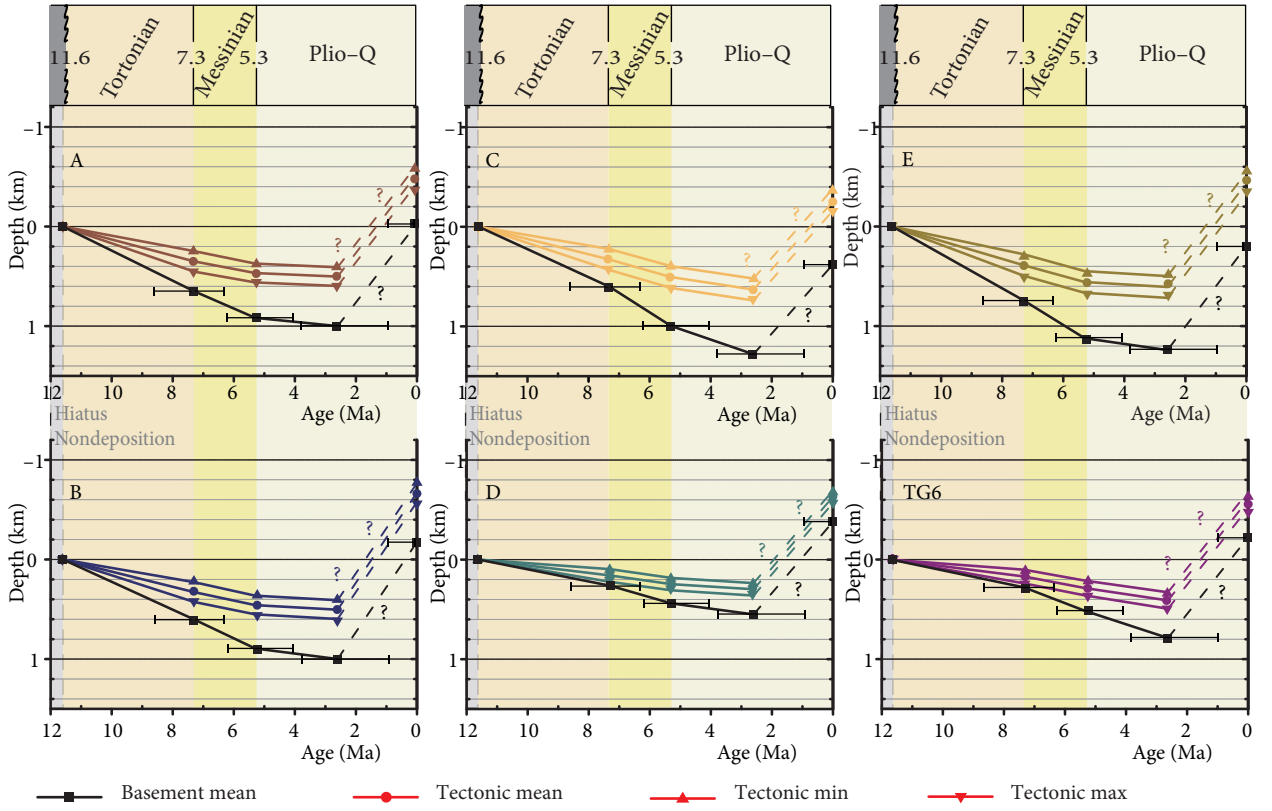

Figure 13. Subsidence curve plots for the synthetic wells (SCS A to E) and the TG6 well (SCS TG6). The location of these sites is shown in Figure 2. The initial topography is assumed to be 0 km in all cases. The upward motion (positive slope) observed in the younger stages was created by including the value of the present-day topography to the curve, thus bringing the curves to their present depths.

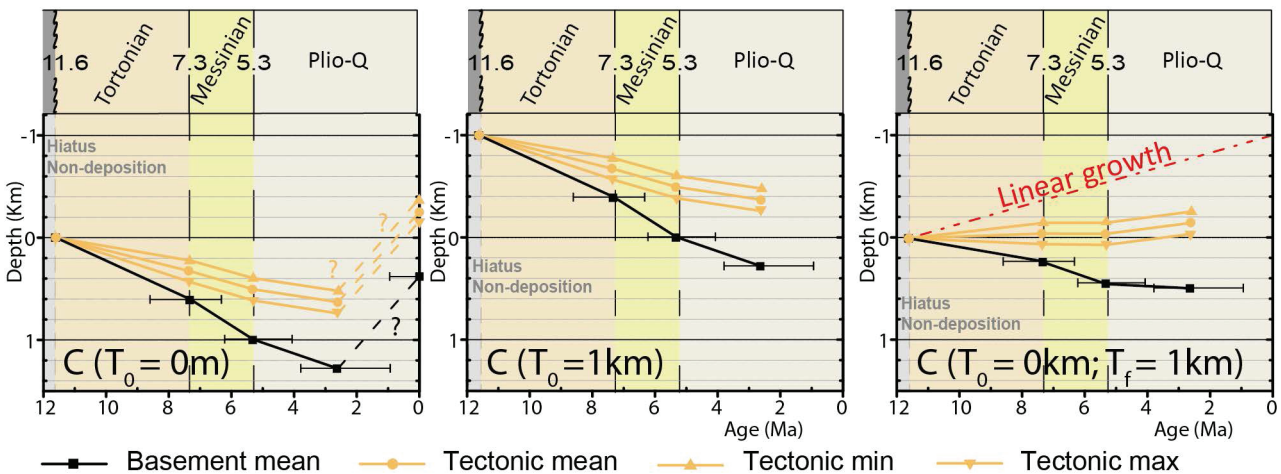

Figure 14. Scenarios of subsidence curves. The left panel is the reference scenario, SCS C, in which the initial topography is considered as 0 km and the younger uplift corresponds to present-day depths of the points in the curve (see Figure 13). The central panel corresponds to a scenario in which the initial palaeoelevation has been considered to be similar to the present topography (1 km) since Tortonian times for SCS C. The panel on the right represents a scenario in which a linear topographic growth is assumed from Tortonian (0 km) to present (1 km) for SCS C.

curves in this scenario represent a situation in which the contribution to subsidence by tectonic forces is minimum or absent and the contribution by sediment loading might be the driving mechanism.

6.2. Horizontal movements

6.2.1. Methodology and data

Based on the assumption of cross-sectional area conservation after deformation of postdepositional sedimentary bodies, balancing of cross-sections is used for geometrical validation of geological interpretations (e.g., Dahlstrom 1969; Elliott 1983). Restoration is a related technique that provides a quantitative analysis of horizontal deformations. Restorations that do not balance show incompatibilities, unrealistic structures, or changes in area that expose errors in seismic interpretation or incorrect restoration parameters (e.g., Schultz-Ela 1992).

The depth-converted seismic line A (Figure 5) was used for restoration. Line A transects at a high angle the major structures accounting for horizontal displacements in the area, is roughly parallel to the transport directions obtained by Özsayın *et al.* (2013), and is in agreement with other studies in surrounding areas (e.g., Koçyiğit 1995). This line was simplified and divided into straight-lined blocks and faults, and faults with horizontal offsets of <50 m were removed. Manual restoration was accomplished using the equal area method described by Mitra and Namson (1989) without key-bed balanced modification. During the restoration, the fault geometries and block sectional areas remained constant. This implies the assumptions of nonpenetrative deformation, absence of pressure-solution events, or lack of bedding-plane slip. The retrodeformation was completed along fixed faults in a sequence opposite to the main transport direction, i.e. from north-east to south-west.

Three different points along the section were used as references to trace horizontal displacements. From north-east to south-west, they are P(r) in the stable area in the east and used as a pin, P(I) on the hanging wall of the SAT sliver, and P(II) on the hanging wall of the Tuz Gölü normal fault in the west (Figure 15).

6.2.2. Restoration procedure

The restoration to pre-Miocene deposition was accomplished in 8 steps by means of simple shear displacement, either vertical or ranging from 45° to 60° opposite the transport direction) (Figure 15; Table 3).

Vertical shear along the end points of the section allowed restoration to a regional datum (from section I to section II in Figure 15). To retrodeform the section to the moment of initial deposition of Unit 1 (from section II to section III in Figure 15), 5 block displacements along faults were performed. First *(1)*, a vertical simple shear along the easternmost part of the section, removed the Pliocene layer. Since the faults used to retrodeform steps *(2)* to *(4)* were transecting the SAT sheet, this structure was used as a reference level. Rotational movements along the faults lead to restoration in *(2)* and *(3)*, and a simple shear of 60° along the fault was restored in step *(4)*. Restoration of the movement along the TGF, step *(5)*, was accomplished by a simple shear of 45° with respect to the horizontal. Retrodeformation to the initial deposition of Unit 2 was achieved from section III to section V, as shown in Figure 15. Since the SAT is cutting Unit 2, the restoration along this fault in step *(6)* should be performed prior to the restoration of deposition of the mentioned unit. A 45° simple shear along the SAT provides the best retrodeformation results. This 45° simple shear was applied individually to each segment of the SAT. An oblique simple shear of 45° along the TGF in step *(7)* retrodeformed Unit 2. The final restoration along the TGF occurred with an oblique simple shear of 45° for Unit 3 in step *(8)* (from section V to section VI), removing the last components of extension in the TGF. The strain values obtained during restoration are shown in Table 3.

6.2.3. Analysis of horizontal motion

A primary analysis of the horizontal displacement along line A shows that this section was 8 km longer than at present before the beginning of deposition of the Unit 3 sediments (Figure 15). During the deposition of Unit 2 (Figure 15, Step 4), the line gained 140 m more in length, due to an extension along the post-Palaeogene TGF. Sometime before deposition of the Unit 1 sediments (Figure 15, Step 3), the emplacement of the SAT led to more than 8 km of contractional horizontal displacement for both P(I) and P(II) with respect to P(r), by far the most important displacement found during restoration. In the younger stages, horizontal displacements along the TGF caused the removal of 120 m of extension, as quantified in the displacement of P(II).

6.2.4. Restoration artefact and vertical motion mismatch

Our restoration of the movement along the SAT to a Late Miocene prebase produced a mismatch with the vertical motions quantified by the subsidence curves. The restoration of line A produced in the south-west part of the TGF (blank area in Figure 15, Step 4) showed a vertical displacement of ~2.8 km. The SCS C, in line B, also located in the hanging wall of the TGF and considered to have a similar evolution, indicated a vertical displacement of ~1.3 km. This difference, produced by our decision to maintain block motion along the SAT, may be a consequence of any or a combination of the following: (i) the SAT transport direction not being north-east, (ii) the overall south-west tilt of the area, and/or (iii) the volume changes caused by compaction, which could account for volume changes of up to 40% (Wood 1981).

We consider that palinspastic restoration is not a technique meant to account for vertical movement, but rather to determine horizontal displacement. Thus, we understand that the primary horizontal signal seen in the restoration is factual. In this manner, here and elsewhere,

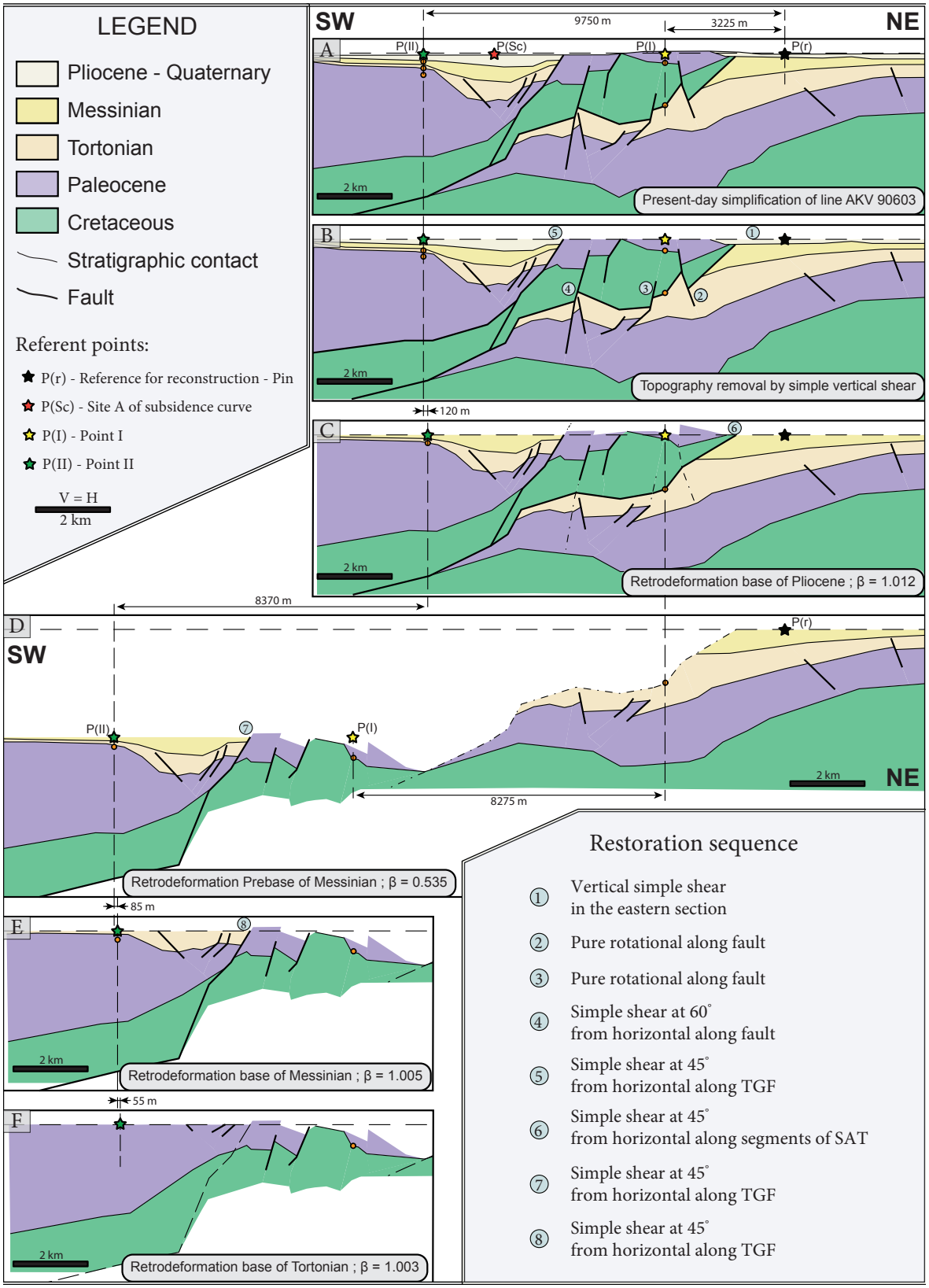

Figure 15. Equal-area restoration of depth-converted line A and removal of each seismic unit for every time-slide until the pre-Tortonian. The restoration sequence was performed in the order shown by the grey numbers both in the sections and in the lower right corner.

Table 3. Horizontal displacements and strain from the restoration. TGF = Tuz Gölü Fault and SAT = Şereflikoçhisar–Aksaray Thrust. P(r) is the point of reference during restoration, and P(I) and P(II) are points located in the front and the back of the thrust. β was obtained by dividing the final length by the initial length when measuring the distances P(r) – P(I) and P(r) – P(II).

	Distance (m) from P(r)		Horizontal deformation*				Restored structures
			Displacement (m)		$\beta = l_1/l_2$		
	P(I)	P(II)	P(I)	P(II)	P(I)	P(II)	
Present	9750	3325	120	0	1.12	1	Small faults / TGF
Base of Pliocene	9630	3325	–8370	–8275	0.535	0.286	SAT
Top of Messinian	18,000	11,600	85	0	1.005	0.286	TGF
Base of Messinian	17,815	11,600	55	0	1.003	1	TGF
Base of Tortonian	17,860	11,600	-	-	-	-	-

*Values represent variations between the former and the previous time-slides.

values for the horizontal motions have been obtained from the restoration and values for the vertical motions from the subsidence curves.

6.3. Comparison of tectonic motions

The horizontal deformation values obtained in the restoration shown in Table 3 are plotted in Figure 16 along with the subsidence curve in SCS C and the estimated periods of activity on the main faults for comparison. No direct relationship can be established between the subsidence curves and the fault activity (see Figure 16). During the beginning of post-Palaeogene times, the initial movements on the TGF assumed 140 m of extension and subsided at about 600 m. Nevertheless, subsidence rates remained constant while subsequent SAT tectonics occurred. In this manner, ~200 m of subsidence is linked with ~8 km of shortening. One probable explanation is that overall subsidence happened in the area independently of the applied stresses. That is, both the extensional and contractional phases occurred in the region while an independent regional subsidence led to 800 m of downward motion.

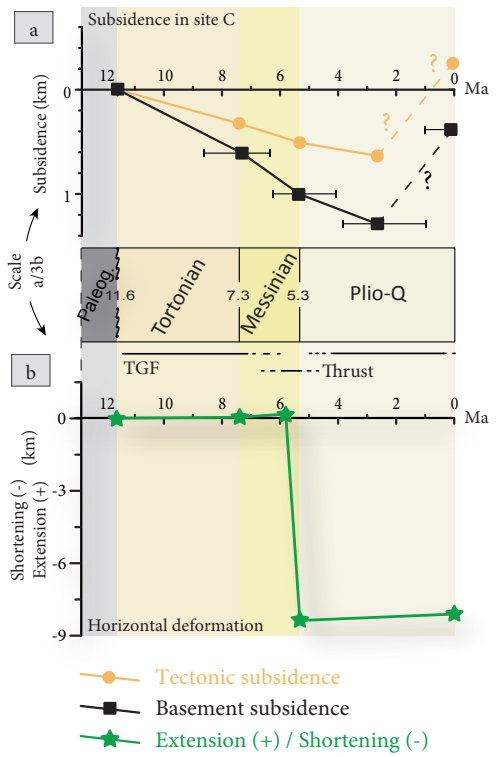

Figure 16. Comparison between the subsidence curve in site C and values obtained during restoration as well as a tentative representation of activity of the main faults through time.

7. Evolution of the Tuz Gölü area: a 3D model

7.1. Late Palaeogene

Overall subsidence began in Maastrichtian times (Görür *et al.* 1984; Çemen *et al.* 1999), leading to the development of a broad sag basin that further developed during the Early Palaeogene. In less than 13 Ma, the area experienced between 1500 m and 2200 m of basement subsidence (Figure 17) with respect to the surroundings. The extent of this basin exceeded the limits of the study area and its formation was not related to the development of basin-forming faults. However, the SFS was active as an extensional or strike-slip intrabasinal fault during this time interval, suggesting at least local extension.

After this subsidence phase, a long period of no deposition took place, which is represented as an unconformity. This period is associated with regional uplift between 40 Ma and 23 Ma (Genç & Yürür 2010 and the references therein) as well as shallowing and sea retreat in Central Anatolia by the end of the Lutetian (Çiner *et al.* 1996; Görür *et al.* 1998).

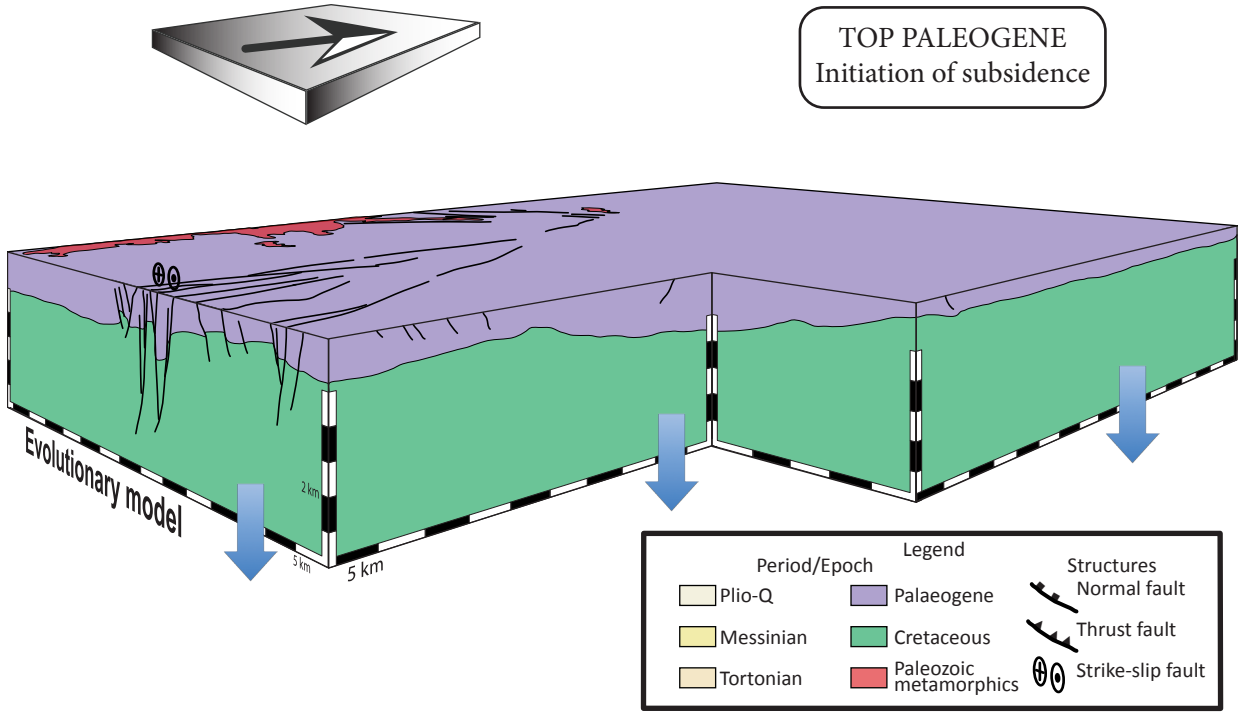

Figure 17. Real-scale box model (exaggerated 3 times in the vertical direction) showing the main tectonic structures and tectonic movements after Palaeogene deposition. Arrows indicate the direction, type, and relative magnitude of the movements.

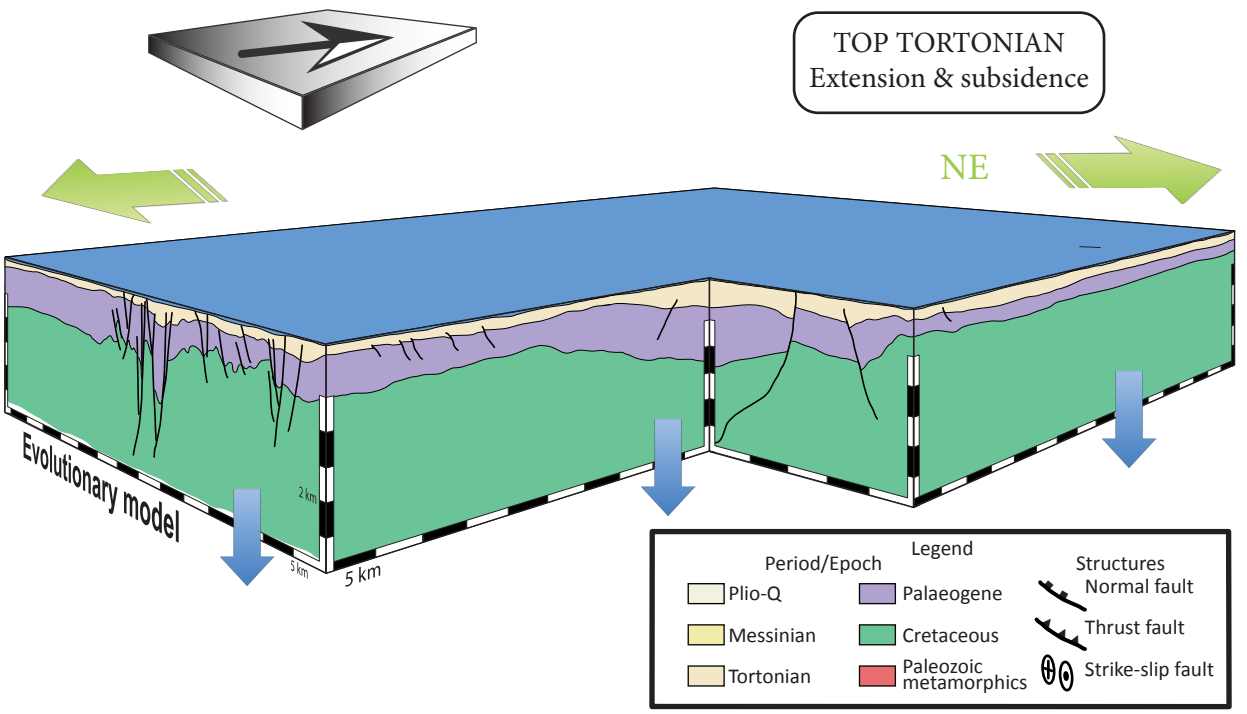

Figure 18. Real-scale box model (exaggerated 3 times in the vertical direction) showing the main tectonic structures and tectonic movements after Tortonian deposition. Arrows indicate the direction, type, and relative magnitude of the movements.

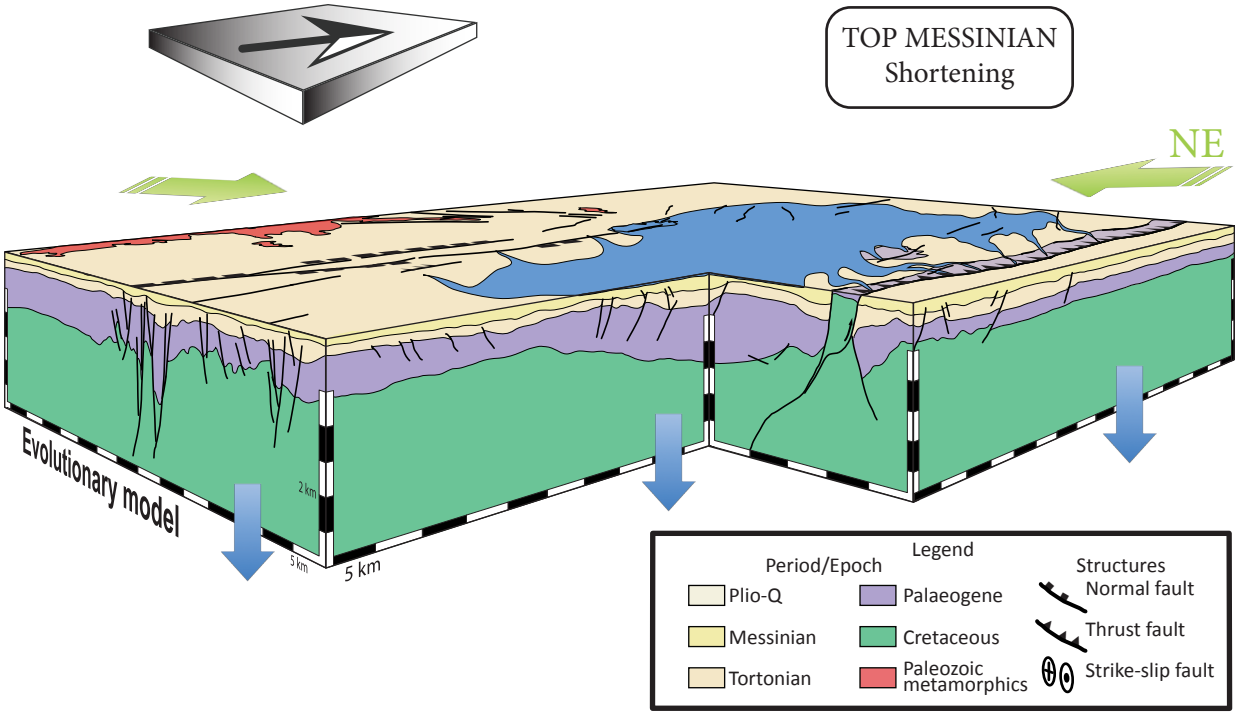

Figure 19. Real-scale box model (exaggerated 3 times in the vertical direction) showing the main tectonic structures and tectonic movements after Messinian deposition. Arrows indicate the direction, type, and relative magnitude of the movements.

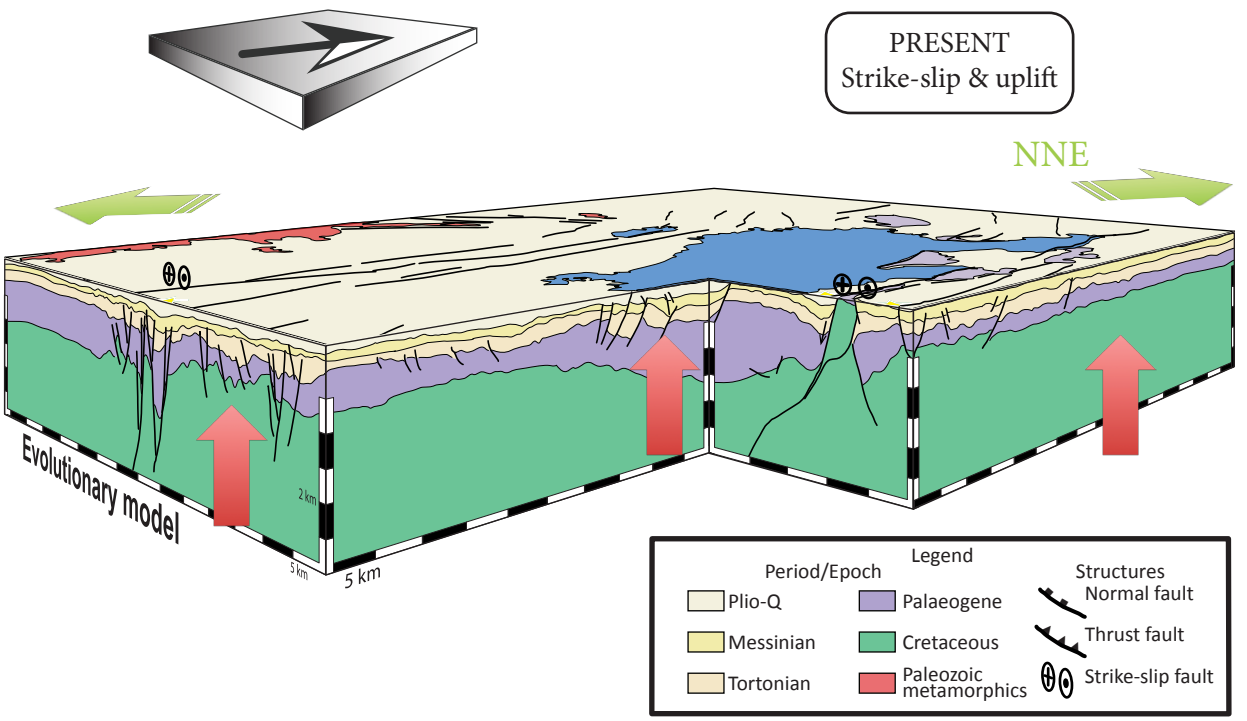

Figure 20. Real-scale box model (exaggerated 3 times in the vertical direction) showing the main tectonic structures and tectonic movements in present times. Arrows indicate the direction, type, and relative magnitude of the movements.

7.2. Late Tortonian

Sedimentation restarted by Tortonian times (Figure 18). The previous regional subsidence in the sag basin changed toward a more structurally (fault) controlled subsidence. Both the TGFS and the SFS were active structures and clearly influenced the sediment distribution in the TGB. Trending in a NW–SE direction, the initial accumulation of sedimentary deposits in the north reached thicknesses of 800 m in relation to 2 extensional faults shaping a horst, namely the TGFS. Syntectonic deposition of Tortonian sediments on each side of this horst took place. The southern depocentre, striking in a NE–SW direction, accumulated more than 900 m of sediments in relation to the SFS, where syntectonic deposition doubled the sedimentary thicknesses.

7.3. Late Messinian

A similar evolution to that occurring in Tortonian times happened in the area during the Messinian (Figure 19). A continuation of the subsidence and local extension led to further narrowing of the depocentres as markedly NNW–SSE oriented, in association with the activity of the TGFS and SFS. The depression related to the SFS accumulated up to 500 m of sediments (relative to the surroundings) during this period. Concurrently, 400 m of sediments were deposited in relation to the TGFS. During this continued subsidence, a final Miocene-Pliocene shortening phase took place. This kinematic changeover resulted in the development of contractional features in the area. The SAR is the most relevant among these structures and was formed by the north-east emplaced SAT sliver, which accounted for more than 8 km of horizontal displacement.

7.4. Present

By the beginning of the deposition of Pliocene sediments (Figure 20), a new extensional phase followed the previous contraction (Çiner *et al.* 2011; Özsayın *et al.* 2013). We observed this on both sides of the TGFS; on the eastern side of the system normal faults offset the SAT, whereas on the western side, a rollover anticline morphology with a harpoon structure was found (Figures 5 and 6). The development of this extensional reactivation accompanied the regional uplift of the area.

8. Discussion

8.1. Extent of the Tuz Gölü Basin

The relevant literature on the area considers the TGFS and the SFS to be Late Cretaceous to Palaeogene basin-forming faults (e.g., Dirik & Göncüoğlu 1996; Derman *et al*. 2000; Dirik & Erol 2000; Özsayın & Dirik 2007; Huvaz 2009). However, this seismo-structural study showed no basin terminations, and thus connection to or disconnection from other areas farther away could not be established.

In the case of the TGFS, our palinspastic restoration demonstrates that this system was not present by Palaeogene times. This interpretation is compatible with the thickness of the Palaeogene sediments, which continuously increases from NE to SE disregarding the younger TGFS. Furthermore, the offsets shown indicate that the initial sedimentation is unrelated to the fault system and only partially affected by it at a later stage, which is at least as late as post-Palaeogene.

The SFS, a southward continuation of the İnönü-Eskişehir Fault System (Özsayın & Dirik 2007), has been considered to be the east-dipping western boundary of the TGB or a fault pair shaping a graben (e.g., Dirik & Erol 2000; Genç & Yürür 2010). However, within the area transected by the seismic lines, the SFS is shown as a south-west dipping fault set. This fault system was possibly present by Late Cretaceous times but created no boundary for the basin (Figure 11). Instead, the SFS was probably acting as an extensional to strike-slip intrabasinal fault (see Figure 17).

Therefore, we consider that the Palaeogene sedimentary deposition during the initial basin formation is related neither to the TGFS nor the SFS and might instead be a consequence of regional sag subsidence.

8.2. Miocene kinematics in the Tuz Gölü Basin

The distribution and cutting relationships of the different fault families found in the TGB show 3 deformation phases. An initial extension during Tortonian times took place after a phase of uplift and erosion (Genç & Yürür 2010). This local extensional phase was concentrated along the TGFS and the SFS and was initiated with the onset of regional subsidence in Central Anatolia. During the continued subsidence, a hitherto undocumented latest Miocene-Pliocene shortening event occurred. This shortening phase is quantitatively almost 2 orders of magnitude larger than the preceding and subsequent extensional phases. This relevant but relatively short contractional period was overprinted by extension in the area, which took place during uplift of the CAP. This extension–shortening–extension succession of events is in contrast with the idea of a continuous Miocene extension (Şengör & Yılmaz 1981; Koçyiğit *et al.* 1995; Genç & Yürür 2010).

8.3. Tectonics of the Tuz Gölü Basin

We found 2 different stages of basin generation, in the Palaeogene and the Late Miocene-Recent. We believe that these phases are unrelated to each other and developed as a consequence of different driving mechanisms.

The sediment geometries and faults found in the study area are in general agreement with the idea of a forearc genesis of the Palaeogene basin (e.g., Görür *et al.* 1984; Koçyiğit *et al.* 1988) and discard its intracratonic formation (Arıkan, 1975). During the Palaeogene, crustal thickening took place in relation to the subduction of the oceanic crust of the Sakarya Continent beneath the Kırşehir Massif, and

a foredeep developed (Görür *et al.* 1984; Koçyiğit *et al.* 1988). This mechanism is in agreement with the geometry of the Palaeogene package, the relatively minor influence of the faults, and the up to 2300 m of basement subsidence found in this study. However, no backthrust structures that might confirm this genetic model were found in the studied area.

The structural evidence found in the Late Miocene-Recent basin suggest that extension was acting prior to the deposition of Unit 2. This extension is nearly coeval with adakitic subduction-related lavas (high Sr/Y and La/Yb ratios) in the Central Anatolia Volcanic Province (Aydar *et al.* 2010). The latest Miocene shortening phase found in this study roughly coincides with the moment of surface uplift in the CAP, recently stated as younger than ~8 Ma for the south of the CAP (Cosentino *et al.* 2012) and Late Miocene to Early Pliocene for the north of the plateau (Yıldırım *et al.* 2011). Considering these simultaneous occurrences of events, we interpret that a major shortening event as young as 7–5 Ma might be the cause behind the formation of the CAP.

8.4. Conclusions

The analysed seismic data indicate a complex evolution for the study area during the Miocene to Present times, in which (i) a regional subsidence phase that started in Tortonian times with the accumulation of more than 800 m of sediments continued through the Late Miocene and possibly well into Pliocene times, and (ii) an extensional phase that initiated with the onset of the subsidence was disrupted by a relevant relatively short contractional period sometime in the latest Miocene-Pliocene, which was subsequently overprinted by extension.

The fact that the vertical motions are not linked directly to the extensional/shortening events is an indication of 2 different types of vertical motions acting simultaneously in the area. A first-order regional movement caused overall subsidence and subsequent surface uplift. Local movements of minor wavelengths appear in relation to the studied structures modulating the first-order motions.

Acknowledgements

We are indebted to the Netherlands Organization for Scientific Research (NWO) and TÜBİTAK (project no: 107Y333) for financial support. We also acknowledge the General Directorate of Petroleum Affairs (TPAO) and Kadir Dirik for providing the seismic sections. The manuscript benefited from the comments of Cenk Yaltırak, Naci Görür, and Bora Rojay. The authors would like to thank Özkan Huvaz for the discussions on the age of the Cihanbeyli formation as well as Alkor Kutluay, Erman Özsayın, and the members of the ESF-sponsored TopoEurope Vertical Anatolian Movement Project (VAMP) for discussions and unpublished information. We are especially thankful to Fabrizio Pepe for providing us with GeoSuite AllWorks®. Special thanks go to Juan Luis Alonso and Josep Poblet for their supportive discussions on restoration; to Piet Gerritsma, Marina Quintero-Pérez, and Liviu Matenco for their valuable input on the processing of seismic velocities; and to Mohamed Gouiza and Javier Fernández-Lozano for their active discussions.

References

Al-Chalabi, M. 1997a. Parameter nonuniqueness in velocity versus depth functions. *Geophysics* **62**, 970–979.

Al-Chalabi, M. 1997b. Time-depth relationships for multilayer depth conversion. *Geophysical Prospecting* **45**, 715–720.

Arıkan, Y. 1975. The geology and petroleum prospects of the Tuz Gölü Basin. *Mineral Research and Exploration Institute of Turkey (MTA) Publications* **85**, 17–37.

Aydar, E., Cubukcu, H.E., Sen, E., Ersoy, O., Duncan, R.A. & Ciner, A. 2010. Timing of Cappadocian volcanic events and its significance on the development of Central Anatolian Orogenic Plateau. *Geophysical Research Abstracts* **1994**, 10147.

Aydemir, A. & Ateş, A. 2005. Preliminary evaluation of Central Anatolian basins in Turkey by using the gravity and magnetic data. *Journal of the Balkan Geophysical Society* **8**, 7–19.

Aydemir, A. & Ateş, A. 2006a. Structural interpretation of the Tuzgolu and Haymana Basins, Central Anatolia, Turkey, using seismic, gravity and aeromagnetic data. *Earth Planets and Space* **58**, 951.

Aydemir, A. & Ateş, A. 2006b. Interpretation of Suluklu-Cihanbeyli-Goloren Magnetic Anomaly, Central Anatolia, Turkey: an integration of geophysical data. *Physics of the Earth and Planetary Interiors* **159**, 167–182.

Aydemir, A. & Ateş, A. 2008. Determination of hydrocarbon prospective areas in the Tuzgolu (Saltlake) Basin, Central Anatolia, by using geophysical data. *Journal of Petroleum Science and Engineering* **62**, 36–44.

Bassant, P., Van Buchem, F., Strasser, A. & Görür, N. 2005. The stratigraphic architecture and evolution of the Burdigalian carbonate-siliciclastic sedimentary systems of the Mut Basin, Turkey. *Sedimentary Geology* **173**, 187–232.

Bessis, F. 1986. Some remarks on the study of subsidence of sedimentary basins: application to the Gulf of Lions margin (Western Mediterranean). *Marine and Petroleum Geology* **3**, 37–63.

Bond, G. & Kominz, M. 1984. Construction of tectonic subsidence curves for the Early Paleozoic miogeocline, southern Canadian Rocky Mountains: implications for subsidence mechanisms, age of break up, and crustal thinning. *Geological Society of America Bulletin* **95**, 155-173.

Bourbie, T., Coussy, O., Zinszner, B. & Junger, M.C. 1992. Acoustics of porous media. *Journal of the Acoustical Society of America* **91**, 30–80.

Çemen, I., Göncüoğlu, M. & Dirik, K. 1999. Structural evolution of the Tuzgölü Basin in Central Anatolia, Turkey. *Journal of Geology* **107**, 693–706.

Çiner, A., Aydar, E., Dirik, K., Rojay, B., Özsayin, E., Ersoy, O., Çubukçu, E., Kutluay, A. & Yildirim, C. 2011. Vertical Anatolian Movement Project. TOPOEUROPE - ESF (European Science Foundation) - *TÜBİTAK Co-Project* No: **107Y333**.

Çiner, A., Deynoux, M., Ricou, S. & Kosun, E. 1996. Cyclicity in the Middle Eocene Çayraz Carbonate Formation, Haymana Basin, Central Anatolia, Turkey. *Paleogeography, Paleoclimatology, Paleoecology* **121**, 313–329.

Çiner, A., Karabıyıkoğlu, M., Monod, O., Deynoux, M. & Tuzcu, S. 2008. Late Cenozoic sedimentary evolution of the Antalya Basin, Southern Turkey. *Turkish Journal of Earth Sciences* **17**, 1–41.

Cosentino, D., Schildgen, T., Cipollari, P., Faranda, C., Gliozzi, E., Hudáčková, N., Lucifora, S. & Strecker, M. 2012. Late Miocene surface uplift of the southern margin of the Central Anatolian Plateau, Central Taurides, Turkey. *Geological Society of America Bulletin* **124**, 133–145.

Dahlstrom, C. 1969. Balanced cross sections. *Canadian Journal of Earth Sciences* **6**, 743–757.

Derman, S., Rojay, B., Güney, H. & Yıldız, M. 2000. Şereflikoçhisar-Aksaray fay zonunun evrimi hakkında yeni sedimantolojik veriler. Haymana-Tuzgölü-Ulukışla Basenleri Uygulamalı Çalışma. *Türkiye Petrol Jeologları Derneği, Özel Sayı* **5**, 47–70 (in Turkish).

Dewey, J.F., Hempton, M.R., Kidd, W.S.F., Şaroğlu, F. & Şengör, A.M.C. 1986. Shortening of continental lithosphere: the neotectonics of Eastern Anatolia – a young collision zone. *In:* Coward, M.P. & Ries, A.C. (eds), *Collision Tectonics*. Geological Society, London, Special Publications (R.M. Shackleton volume) **19**, 3–36.

Dirik, K. & Erol, O. 2000. Tuzgölü ve civarının tektonomorfolojik evrimi [Tectonomorphologic evolution of Tuzgölü and surrounding area]. Haymana-Tuzgölü-Ulukıflla Basenleri Uygulamalı Çalışma. *Türkiye Petrol Jeologları Derneği, Özel Sayı* **5**, 27–46 (in Turkish with English abstract).

Dirik, K. & Göncüoğlu, M. 1996. Neotectonic characteristics of central Anatolia. *International Geology Review* **38**, 807–817.

Dix, C.H. 1955. Seismic velocities from surface measurements. *Geophysics* **20**, 68–86.

Ducea, M. 2011. Fingerprinting orogenic delamination. *Geology* **39**, 191–192.

Elliott, D. 1983. The construction of balanced cross-sections. *Journal of Structural Geology* **5**, 101–115.

Eriş, K.K., Bassant, P. & Ülgen, U.B. 2005. Tectono-stratigraphic evolution of an Early Miocene incised valley-fill (Derinçay Formation) in the Mut Basin, Southern Turkey. *Sedimentary Geology* **173**, 151–185.

Etris, E., Crabtree, N., Dewar, J. & Pickford, S. 2001. True depth conversion: more than a pretty picture. *CSEG Recorder* **11**, 11–22.

Genç, Y. & Yürür, M.T. 2010. Coeval extension and compression in Late Mesozoic-Recent thin-skinned extensional tectonics in Central Anatolia, Turkey. *Journal of Structural Geology* **32**, 623–640.

Göğüs, O.H. & Pysklywec, R.N. 2008. Near-surface diagnostics of dripping or delaminating lithosphere. *Journal of Geophysical Research* **113**, 1–11.

Görür, N., Oktay, F., Seymen, İ. & Şengör, A.M.C. 1984. Palaeotectonic evolution of the Tuzgolu basin complex, Central Turkey: sedimentary record of a Neo-Tethyan closure. *Geological Society, London, Special Publications* **17**, 467–482.

Görür, N., Tüysüz, O. & Şengör, A.M.C. 1998. Tectonic evolution of the central Anatolian basins. *International Geology Review* **40**, 831–850

Gürbüz, C. & Evans, J.R. 1991. A seismic refraction study of the western Tuz Gölü basin, central Turkey. *Geophysical Journal International* **106**, 239–251.

Hüsing, S.K., Zachariasse, W.J., van Hinsbergen, D.J.J., Krijgsman, W., Inceoz, M., Harzhauser, M., Mandic, O. & Kroh, A. 2009. Oligocene-Miocene basin evolution in SE Anatolia, Turkey: constraints on the closure of the eastern Tethys gateway. *Geological Society, London, Special Publications* **311**, 107–132.

Huvaz, O. 2009. Comparative petroleum systems analysis of the interior basins of Turkey: implications for petroleum potential. *Marine and Petroleum Geology* **26**, 1656–1676.

Huw Davies, J. & von Blanckenburg F. 1995. Slab breakoff: a model of lithosphere detachment and its test in the magmatism and deformation of collisional orogens. *Earth and Planetary Science Letters* **129**, 85–102.

Jaffey, N. & Robertson, A. 2005. Non-marine sedimentation associated with Oligocene-Recent exhumation and uplift of the Central Taurus Mountains, S Turkey. *Sedimentary Geology* **173**, 53–89.

Keskin, M. 2003. Magma generation by slab steepening and breakoff beneath a subduction-accretion complex: an alternative model for collision-related volcanism in Eastern Anatolia, Turkey. *Geophysical Research Letters* **30**, 8046.

Koçyiğit, A., Özkan, S. & Rojay, B.F. 1988. Examples from the fore-arc basin remnants at the active margin of northern Neotethys; development and emplacement age of the Anatolian Nappe, Turkey. *Middle East Technical University Journal of Pure and Applied Sciences* **21**, 183–220.

Koçyiğit, A., Türkmenoğlu. A., Beyhan, A., Kaymakçi, N. & Akyol, E. 1995. Post-collisional tectonics of Eskişehir-Ankara-Çankiri segment of Izmir-Ankara-Erzincan Suture Zone (IAESZ): Ankara Orogenic Phase. *Bulletin of the Turkish Association of Petroleum Geology* **6**, 69–86.

Mavko, G., Mukerji, T. & Dvorkin, J. 2003. *The Rock Physics Handbook: Tools for Seismic Analysis of Porous Media*. Cambridge University Press, Cambridge.

Mitra, S. & Namson, J. 1989. Equal-area balancing. *American Journal of Science* **289**, 563–599.

Okay, A.I. & Tüysüz, O. 1999. Tethyan sutures of northern Turkey. *Geological Society, London, Special Publications* **156**, 475–515.

Okay, A.I., Zattin, M. & Cavazza, W. 2010. Apatite fission-track data for the Miocene Arabia-Eurasia collision. *Geology* **38**, 35–38.

Önal, K., Büyüksaraç, A., Aydemir, A. & Ateş, A. 2008. Investigation of the deep structure of the Sivas Basin (innereast Anatolia, Turkey) with geophysical methods. *Tectonophysics* **460**, 186–197.

Özsayın, E., Çiner, A., Rojay, B.F., Dirik, K., Melnick, D., Fernández-Blanco, D., Bertotti, G., Schildgen, T.F., Garcin, Y., Strecker, M. & Sudo, M. 2013. Plio-Quaternary extensional tectonics of the Central Anatolian Plateau: a case study from the Tuz Gölü Basin, Turkey. "Late Cenozoic Evolution of the Central Anatolia Plateau" In: Çiner, A., Strecker, M. & Bertotti, G. (eds), *Turkish Journal of Earth Sciences* **22**, 691–714.

Özsayın, E. & Dirik, K. 2007. Quaternary activity of the Cihanbeyli and Yeniceoba Fault Zones: İnönü-Eskisehir Fault System, Central Anatolia. *Turkish Journal of Earth Sciences* **16**, 471–492.

Özsayın, E. & Dirik, K. 2011. The role of oroclinal bending in the structural evolution of the Central Anatolian Plateau: evidence of a regional changeover from shortening to extension. *Geologica Carpathica* **62**, 345–359.

Reilly, J. 1993. Integration of well and seismic data for 3D velocity model building. *First Break* **11**, 247–260.

Robertson, A.H.F. 1998. Mesozoic-Tertiary tectonic evolution of the easternmost Mediterranean area: integration of marine and land evidence. *In*: *Proceedings of the Ocean Drilling Program. Scientific Results*. Ocean Drilling Program **160**, 723–782.

Robinson, A.H.F., Spadini, G., Cloetingh, S. & Rudat, J. 1995. Stratigraphic evolution of the Black Sea: inferences from basin modeling. *Marine and Petroleum Geology* **12**, 821–835.

Rojay, B.F. 1995. Post-Triassic evolution of Central Pontides: evidence from Amasya region, northern Anatolia. *Geologica Romana* **31**, 329–350.

Şafak, U., Kelling, G., Gökçen, N.S. & Gürbüz, K. 2005. The mid-Cenozoic succession and evolution of the Mut basin, southern Turkey, and its regional significance. *Sedimentary Geology* **173**, 121–150.

Schultz-Ela, D.D. 1992. Restoration of cross-sections to constrain deformation processes of extensional terranes. *Marine and Petroleum Geology* **9**, 372–388.

Sclater, J. & Christie, P. 1980. Continental stretching: an explanation of the post-mid-Cretaceous subsidence of the central North Sea basin. *Journal of Geophysical Research* **85**, 3711–3739.

Şengör, A.M.C. & Yılmaz, Y. 1981. Tethyan evolution of Turkey: a plate tectonic approach. *Tectonophysics* **75**, 181–190.

Şengör, A.M.C., Satir, M. & Akkök, R. 1984. Timing of tectonic events in the Menderes Massif, western Turkey: implications for tectonic evolution and evidence for Pan-African basement in Turkey. *Tectonics* **3**, 693–707.

Steckler, M. & Watts, A. 1978. Subsidence of the Atlantic-type continental margin off New York. *Earth and Planetary Science Letters* **41**, 1–13.

Uğurtaş, G. 1975. Geophysical interpretation of part of the Tuz Gölü Basin. *Mineral Research and Exploration Institute of Turkey (MTA) Publications* **85**, 38–45.

Williams, G.D., Ünlügenç, U.C., Kelling, G. & Demirkol, C. 1995. Tectonic controls on stratigraphic evolution of the Adana Basin, Turkey. *Journal of the Geological Society* **152,** 873–882.

Wood, R. 1981. The subsidence history of Conoco well 15/30-1, central North Sea. *Earth and Planetary Science Letters* **54**, 306–312.

Yıldırım, C., Schildgen, T.F., Echtler, H., Melnick, D. & Strecker, M. 2011. Late Neogene and active orogenic uplift in the Central Pontides associated with the North Anatolian Fault: implications for the northern margin of the Central Anatolian Plateau, Turkey. *Tectonics* **30**, TC5005.